

Large-Scale Bayesian Structure Learning for Gaussian Graphical Models Using Marginal Pseudo-Likelihood

Reza Mohammadi, Marit Schoonhoven, Lucas Vogels and Ş. İlker Birbil
Department of Business Analytics, Faculty of Economics and Business,
University of Amsterdam

July 23, 2024

Abstract

Bayesian methods for learning Gaussian graphical models offer a comprehensive framework that addresses model uncertainty and incorporates prior knowledge. Despite their theoretical strengths, the applicability of Bayesian methods is often constrained by computational demands, especially in modern contexts involving thousands of variables. To overcome this issue, we introduce two novel Markov chain Monte Carlo (MCMC) search algorithms with a significantly lower computational cost than leading Bayesian approaches. Our proposed MCMC-based search algorithms use the marginal pseudo-likelihood approach to bypass the complexities of computing intractable normalizing constants and iterative precision matrix sampling. These algorithms can deliver reliable results in mere minutes on standard computers, even for large-scale problems with one thousand variables. Furthermore, our proposed method efficiently addresses model uncertainty by exploring the full posterior graph space. We establish the consistency of graph recovery, and our extensive simulation study indicates that the proposed algorithms, particularly for large-scale sparse graphs, outperform leading Bayesian approaches in terms of computational efficiency and accuracy. We also illustrate the practical utility of our methods on medium and large-scale applications from human and mice gene expression studies. The implementation supporting the new approach is available through the R package `BDgraph`.

Keywords: Markov random field; Model selection; Link prediction; Network reconstruction; Bayes factor.

1 Introduction

In statistical modeling, graphical models (Lauritzen, 1996; Koller and Friedman, 2009) stand out as a principal tool for assessing conditional dependencies among variables. Conditional dependence denotes the relationship between two or more variables with the effect of other variables removed. These conditional dependencies are elegantly portrayed using

graphs, where nodes represent random variables (Lauritzen, 1996). Within the context of undirected graphs, the absence of an edge between two nodes implies conditional independence between the variables they represent (Rue and Held, 2005). Estimating that underlying graph structure is called *structure learning*.

In this article, we consider Bayesian structure learning approaches for estimating Gaussian graphical models (GGMs), in contrast with frequentist techniques like the lasso-based neighborhood selection that commonly optimize the likelihood function (Friedman et al., 2008; Peng et al., 2009; Meinshausen and Bühlmann, 2006). The strength of Bayesian approaches lies in handling model uncertainty through posterior distributions and accommodating prior knowledge. Yet, with increasing dimensions, Bayesian methods often lag in computational speed and scalability relative to frequentist alternatives.

The primary objective of Bayesian structure learning methods is to determine the underlying graph structure given the data (Vogels et al., 2023). Bayesian paradigms can achieve this by computing the posterior distribution of the graph conditional on the data. For the case of GGMs, this requires the calculation of a complex integral, a task that becomes increasingly challenging, or even impractical, for larger-scale graphs. Thus, most Bayesian methods (Mohammadi et al., 2023; van den Boom et al., 2022; Peterson et al., 2015; Niu et al., 2023) compute the joint posterior distribution of the graph and precision matrix.

A comprehensive exploration of the joint posterior distribution is feasible only for very small graphs (with a maximum of 10 nodes). This limitation arises because the number of possible graphical models increases at a super-exponential rate with the number of nodes. Consequently, most Bayesian methods employ sampling algorithms over the joint space of graphs and precision matrices, primarily using MCMC sampling. Green (1995) proposed the reversible jump MCMC, which is based on a discrete-time Markov chain. Dobra et al. (2011) implemented this reversible jump MCMC sampling for GGMs. Deriving the joint posterior distribution requires the prior distribution of the precision matrix given the graph. Most Bayesian methods for Gaussian likelihood commonly use a G -Wishart distribution (Roverato, 2002; Letac and Massam, 2007) as a natural conjugate prior for the precision matrix. A computationally expensive step within the search algorithm is determining the ratio of prior normalizing constants for the G -Wishart distribution (Mohammadi et al., 2023). Advancements in reducing calculation time have been suggested by Wang and Li (2012), Cheng and Lenkoski (2012), and Mohammadi et al. (2023). Furthermore, Lenkoski (2013) and Hinne et al. (2014) proposed computationally efficient algorithms to sample from the G -Wishart distribution. Additional efficiency was achieved by Mohammadi and Wit (2015), who proposed a search algorithm known as the birth-death MCMC algorithm, based on a continuous-time Markov chain, to explore the graph space more efficiently. More recently, van den Boom et al. (2022) developed a G -Wishart weighted proposal algorithm featuring delayed acceptance MCMC and an informed proposal distribution on the graph space to reduce computing costs. As an alternative to methods reliant on the G -Wishart prior, Wang (2015) introduced a block Gibbs algorithm using a continuous spike-and-slab prior distribution (Tadesse and Vannucci, 2021). This approach enables the updating of entire columns of the precision matrix, resulting in faster convergence of the MCMC algorithm.

The computational challenge of existing MCMC-based search algorithms lies in their evaluation of the joint posterior distribution of both the graph and precision matrix, rather

than focusing solely on the posterior distribution of the graph. During each MCMC iteration, these algorithms encounter two main computational issues: (i) the difficult-to-compute normalizing constants that require approximation, and (ii) the update of the precision matrix. Consequently, existing MCMC-based methods become computationally expensive from 100 variables upward for the reversible jump and birth-death MCMC algorithms, and from 250 variables upward for the spike-and-slab approach introduced by Wang (2015). These computational costs restrict the applicability of Bayesian methods in modern applications involving thousands of variables. Thus, to handle large-scale graphical models, some form of approximation is inevitable.

The main contribution of this article is the introduction of a novel MCMC-based methodology for GGMs. Rather than focusing on the joint posterior distribution of the graph and the precision matrix, we concentrate solely on the posterior distribution of the graph. Our approach replaces the Gaussian likelihood function with a pseudo-likelihood, which is a product of conditional likelihood functions (Besag, 1975). This allows us to bypass the challenges associated with constant normalization and repeated precision matrix sampling. We introduce two MCMC-based search algorithms that leverage the marginal pseudo-likelihood (MPL) approach for enhanced computational efficiency.

The concept of substituting the likelihood function with a pseudo-likelihood function is well-established (Varin et al., 2011). These approaches have been adapted for various graphical models (Jalali et al., 2020, 2023; Niu et al., 2023; Atchadé, 2019; Khare et al., 2015; Ji and Seymour, 1996; Ravikumar et al., 2010; Niu et al., 2023). Previous studies, such as those by Pensar et al. (2017) and Dobra and Mohammadi (2018), have applied MPL to undirected graphical models with discrete variables. Similar MPL approaches were implemented by Consonni and Rocca (2012) and Carvalho and Scott (2009) in GGMs but were limited to decomposable graphs. Leppä-aho et al. (2017) extended this approach to non-decomposable graphs by implementing a score-based hill-climbing algorithm. This method is constrained to estimating the maximum a posteriori probability, focusing on the posterior mode rather than the full posterior distribution. Recently, Jalali et al. (2020) developed a scalable Bayesian approach by leveraging the regression-based generalized likelihood function proposed by Khare et al. (2015) and incorporating it with a discrete spike-and-slab prior distribution (Tadesse and Vannucci, 2021). This approach avoids the need to compute normalizing constants but still requires updating the precision matrix, which is done using Gibbs sampling element-by-element. As a state-of-the-art approach, we have compared its performance against our proposed algorithms in the extensive simulation study presented in Section 5.

To demonstrate the computational efficiency and graph recovery precision of our proposed MCMC-based search algorithms, we refer to Figure 1. This plot presents the convergence of the Area Under the Precision-Recall Curve (AUC-PR) over running time for our proposed MCMC-based algorithms (BD-MPL and RJ-MPL) compared with state-of-the-art Bayesian methods. This simulation is for a Cluster graph structure with 1000 nodes, an edge density of 0.5%, and 1050 observations. This visualization is part of our extensive simulation study in Section 5. The figure clearly shows the significantly faster convergence of our proposed MCMC-based algorithm (BD-MPL) compared to leading Bayesian methods, such as the SS method (Wang, 2015), the BD method (Mohammadi and Wit, 2015; Mohammadi et al., 2023), and the B-CONCORD method (Jalali et al., 2020). The plot indicates that the BD-MPL algorithm quickly achieves impressive AUC-PR values (exceed-

ing 0.8) in less than 10 minutes. In contrast, the B-CONCORD algorithm takes around half an hour to reach a decent AUC-PR and fails to reach a comparable level even over one day. The SS algorithm requires an entire day to reach a reasonable AUC-PR and still does not achieve a comparable level. The BD algorithm struggles with such large-scale graphs, remaining near an AUC-PR of approximately 0.0 even after a couple of days.

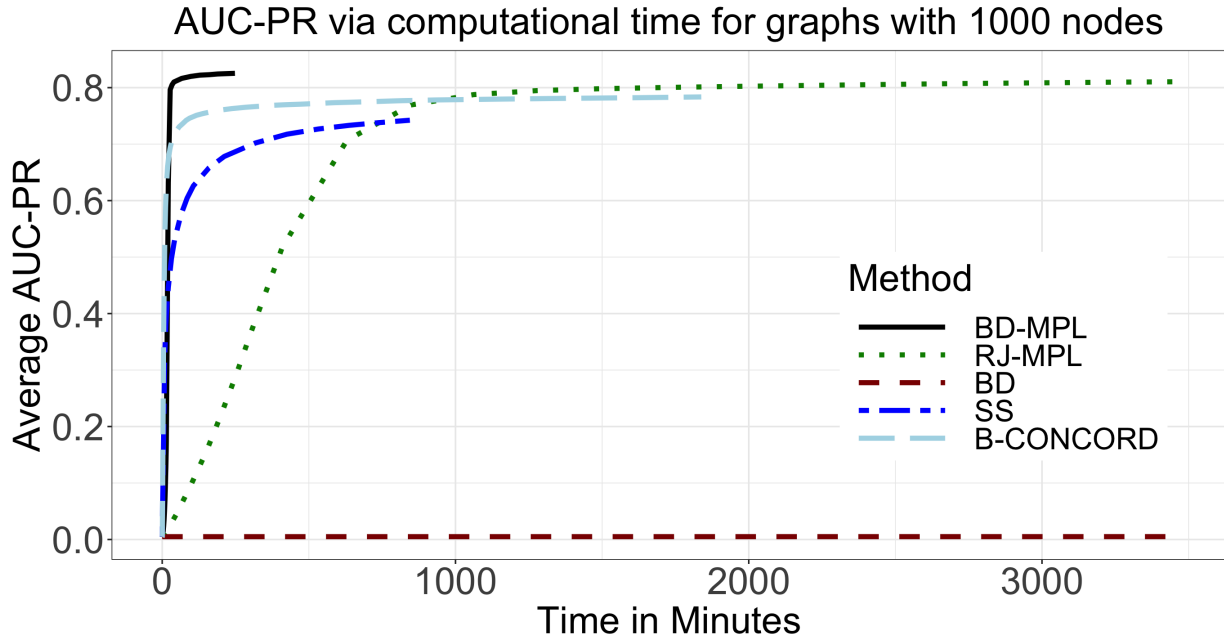


Figure 1: *The convergence of AUC-PR over running time for all algorithms on a Cluster graph with 1000 nodes, 0.5% edge-density, and 1050 observations. BD-MPL and RJ-MPL refer to our proposed MCMC-based search algorithms (Algorithms 1 and 2, respectively). SS represents the Bayesian method presented by Wang (2015). BD stands for the birth-death MCMC search algorithm developed by Mohammadi and Wit (2015) and Mohammadi et al. (2023). B-CONCORD denotes the Bayesian approach developed by Jalali et al. (2020). The plot presents the average AUC-PR values over 8 replications, as part of the simulation study in Section 5.*

The article is organized as follows. Section 2 delves into the fundamental concepts of Bayesian structure learning for GGMs. Section 3 details the MPL approach along with the two proposed MCMC-based search algorithms for large-scale graph recovery. Section 4 discusses the theoretical properties of the proposed algorithms, including convergence proof (Lemma 1), posterior contraction (Lemma 2), and graph selection consistency (Theorem 1). In Section 5, we present a comprehensive simulation study to assess the efficacy of these new algorithms compared to current leading Bayesian methods. Additionally, in Section 6, we evaluate graph recoveries by various methods using two real-world examples: Human gene expression data in Subsection 6.1 and gene expression in immune cells in Subsection 6.2, demonstrating the strengths of the proposed algorithms on both classical medium-scale and large-scale data sets, respectively. We conclude with reflections and potential avenues for future exploration. Our implementation is included in the R package `BDgraph`, available at <http://cran.r-project.org/packages=BDgraph>.

2 Bayesian Structure Learning for GGMs

We denote an undirected graph by $G = (V, E)$, where V contains p nodes corresponding to the p variables and the set of edges is denoted by $E \subset \{(i, j) | 1 \leq i < j \leq p\}$. In this notation, the edge (i, j) denotes the link between nodes i and j . Here, each node represents a distinct random variable. All nodes together form a p -dimensional random vector. We have a data matrix $\mathbf{X} = (\mathbf{X}^{(1)}, \dots, \mathbf{X}^{(n)})^T$ of dimensions $n \times p$. The independent samples/rows, $\mathbf{X}^{(k)}$ for $k \in \{1, \dots, n\}$, correspond to p -dimensional random vectors. In GGMs, each $\mathbf{X}^{(k)}$ is distributed according to a multivariate Gaussian distribution $\mathcal{N}_p(\mathbf{0}, \Sigma)$ with Σ being the covariance matrix. The corresponding precision matrix is denoted by $\mathbf{K} = \Sigma^{-1}$ with elements K_{ij} . Nodes i and j are conditionally independent if and only if $K_{ij} = 0$ (Lauritzen, 1996).

In Bayesian structure learning, the ultimate aim is to estimate the posterior probability of the graph G conditional on the data \mathbf{X} :

$$P(G|\mathbf{X}) \propto P(\mathbf{X}|G)P(G), \quad (1)$$

where $P(G)$ is a prior distribution on the graph-space \mathcal{G}_p of undirected graphs with p nodes and $P(\mathbf{X}|G)$ is the marginal likelihood of graph G .

For the prior distribution of the graph, one can assign constant probabilities denoted by $\beta_{ij} \in (0, 1)$, for including each edge $e = (i, j)$ in G . If all β_{ij} values are set equal to $\beta \in (0, 1)$, it leads to the following prior distribution

$$P(G) \propto \beta^{|E|}(1 - \beta)^{|\bar{E}|}, \quad (2)$$

where $|E|$ denotes the size of set E (the number of edges in the graph G), and \bar{E} denotes the set of edges that are not in G . For sparser graphs, a lower value of β is recommended. When $\beta = 0.5$, the prior becomes non-informative and uniformly distributed over the graph space. It is important to note that our Bayesian framework is not limited to this prior and can accommodate any prior distribution on G . For other choices of priors for graph G , we refer to Dobra et al. (2011); Jones et al. (2005); Mohammadi and Wit (2015); Scutari (2013).

For the marginal likelihood of G , we have

$$P(\mathbf{X}|G) = \int_{\mathbf{K}} P(\mathbf{X}|G, \mathbf{K})P(\mathbf{K}|G)d\mathbf{K}, \quad (3)$$

where $P(\mathbf{K}|G)$ denotes the prior for \mathbf{K} given G and $P(\mathbf{X}|G, \mathbf{K})$ is the likelihood function.

A well-defined choice for the prior distribution of the precision matrix \mathbf{K} is the G -Wishart distribution (Roverato, 2002; Letac and Massam, 2007), which serves as the conjugate prior for the multivariate Gaussian likelihood. The G -Wishart density is

$$P(\mathbf{K}|G) = \frac{1}{I_G(b, \mathbf{D})} |\mathbf{K}|^{\frac{b-2}{2}} \exp \left\{ \frac{-1}{2} \text{tr}(\mathbf{K}\mathbf{D}) \right\} \mathbf{1}(\mathbf{K} \in P_G), \quad (4)$$

where $|\mathbf{K}|$ denotes the determinant of \mathbf{K} , $\text{tr}(\mathbf{A})$ is the trace of a square matrix \mathbf{A} , P_G is the set of positive definite matrices \mathbf{K} with $K_{ij} = 0$ if $(i, j) \notin E$, and $\mathbf{1}(\mathbf{K} \in P_G)$ is an indicator function that equals 1 if $\mathbf{K} \in P_G$ and 0 otherwise.

We denote this distribution with $W_G(b, \mathbf{D})$, where the symmetric positive definite matrix \mathbf{D} and the scalar $b > 2$ are the scale and the shape parameters of the G -Wishart distribution, respectively. Here, $I_G(b, \mathbf{D})$ is the normalizing constant, which is given by

$$I_G(b, \mathbf{D}) = \int_{\mathbf{K} \in P_G} |\mathbf{K}|^{\frac{b-2}{2}} \exp \left\{ \frac{-1}{2} \text{tr}(\mathbf{K}\mathbf{D}) \right\} d\mathbf{K}.$$

Using the G -Wishart prior, Equation 3 becomes

$$P(\mathbf{X}|G) = (2\pi)^{-\frac{np}{2}} \frac{I_G(b+n, \mathbf{D} + \mathbf{U})}{I_G(b, \mathbf{D})},$$

where $\mathbf{U} = \mathbf{X}^T \mathbf{X}$. This ratio of normalizing constants is hard to calculate (Atay-Kayis and Massam, 2005; Mohammadi et al., 2023; Uhler et al., 2018). Therefore most Bayesian structure learning methods approximate it by utilizing MCMC sample algorithms over the joint space of graphs and precision matrices.

The joint posterior distribution of the graph G and the precision matrix \mathbf{K} is given by

$$\begin{aligned} P(G, \mathbf{K}|\mathbf{X}) &\propto P(\mathbf{X}|\mathbf{K}, G)P(\mathbf{K}|G)P(G) \\ &\propto P(G) \frac{1}{I_G(b, \mathbf{D})} |\mathbf{K}|^{\frac{b+n-2}{2}} \exp \left\{ \frac{-1}{2} \text{tr}(\mathbf{K}(\mathbf{D} + \mathbf{U})) \right\}. \end{aligned} \quad (5)$$

Computing the above joint posterior distribution becomes computationally infeasible for $p > 10$ due to the exponential growth in the number of potential graphs. To estimate $P(G, \mathbf{K}|\mathbf{X})$, most Bayesian structure learning methods employ MCMC-based search algorithms. A well-known sampling algorithm for GGMs is the reversible jump MCMC algorithm (Green, 1995), which is based on a discrete-time Markov chain and is commonly utilized in Gaussian graphical models (Dobra et al., 2011; Lenkoski and Dobra, 2011; Cheng and Lenkoski, 2012; Lenkoski, 2013; Hinne et al., 2014). During each MCMC iteration $s \in \{1, \dots, S\}$, the state of the Markov chain is denoted by $(G^{(s)}, \mathbf{K}^{(s)})$, and the chain transitions to the state $(G^{(s+1)}, \mathbf{K}^{(s+1)})$. For a sufficiently large number of iterations S , the distribution of the sample pairs $\left\{ (G^{(1)}, \mathbf{K}^{(1)}), \dots, (G^{(S)}, \mathbf{K}^{(S)}) \right\}$ approximates the posterior distribution $P(G, \mathbf{K}|\mathbf{X})$. The reversible jump MCMC algorithm explores the graph space by adding or removing one edge per iteration. In each iteration, a new graph G' is proposed by modifying the current graph G by adding or removing an edge. A transition to the proposed graph G' is subsequently accepted with a probability given by

$$\alpha(G, G') = \min \left\{ \frac{P(G', \mathbf{K}'|\mathbf{X})}{P(G, \mathbf{K}|\mathbf{X})}, 1 \right\}.$$

This requires computing the ratio of posterior probabilities which can be considered as the conditional Bayes factor for two adjacent graphs. The primary computational challenge for many search algorithms is determining this ratio. To compute this ratio, the following computationally expensive ratio of normalizing constants needs to be determined

$$\frac{I_{G^{(s+1)}}(b, \mathbf{D})}{I_{G^{(s)}}(b, \mathbf{D})}. \quad (6)$$

Given the new graph $G^{(s+1)}$, a new precision matrix $\mathbf{K}^{(s+1)}$ needs to be derived by sampling from the $G^{(s+1)}$ -Wishart distribution. This step is also computationally expensive. Following the introduction of the reversible jump MCMC for Bayesian structure learning, numerous enhancements have been suggested to minimize its high computational demand. Approximations for the ratio of normalizing constants in Equation 6 were presented by Wang (2012), Cheng and Lenkoski (2012), and Mohammadi et al. (2023). Lenkoski (2013) proposed an effective sampling technique designed to reduce the time needed to sample from the G -Wishart distribution. Hinne et al. (2014) leveraged techniques rooted in conditional Bayes factors to cut down on computational time. More recently, van den Boom et al. (2022) introduced the G -Wishart weighted proposal method to improve MCMC mixing and reduce computational cost.

The reversible jump algorithms often suffer from low acceptance rates, requiring more MCMC iterations to converge. To overcome this issue, Mohammadi and Wit (2015) proposed an alternative MCMC-based search algorithm rooted in a continuous-time Markov chain process. This search algorithm explores the graph space by jumping to neighboring graphs. Each jump removes or adds an edge. The jumps are birth-death events that are modeled as independent Poisson processes. Consequently, the time between successive events follows an exponential distribution. In every state $(G^{(s)}, \mathbf{K}^{(s)})$, the chain spends a *waiting time* in that state before it jumps to a new state $(G^{(s+1)}, \mathbf{K}^{(s+1)})$. Once a substantial number of jumps have been made, the samples $(G^{(s)}, \mathbf{K}^{(s)})$, weighted by their respective waiting times, serve as an approximation to the posterior distribution $P(G, \mathbf{K}|\mathbf{X})$.

Despite these improvements, reversible jump and birth-death search algorithms still require significant computational time. This is primarily due to the necessity of sampling a precision matrix from the G -Wishart distribution at each iteration and the fact that the graph changes by at most one edge during each iteration. To address these challenges, Wang (2015) proposed a block Gibbs sampler using a continuous spike-and-slab prior, which facilitates the development of an MCMC algorithm capable of updating entire columns of \mathbf{K} in each iteration. More recently, Jalali et al. (2020) developed a scalable Bayesian approach based on a discrete spike-and-slab prior and a regression-based generalized likelihood function. However, even with these advancements, these algorithms still face computational challenges with large-scale graphs. This is primarily due to the continual need to sample from the precision matrix in every iteration, as pointed out by Vogels et al. (2023) and demonstrated in our simulation study in Section 5.

3 Bayesian Structure Learning with Marginal Pseudo-Likelihood

We introduce two novel MCMC-based search algorithms by using the marginal pseudo-likelihood (MPL) approach. This is explored in conjunction with birth-death and reversible jump MCMC algorithms. In Section 3.1, we illustrate how the MPL approach facilitates the derivation of Bayes factors for MCMC search algorithms. The birth-death and reversible jump MCMC-based search algorithms are detailed in Sections 3.2 and 3.3, respectively.

Recall that we aim to reduce computational cost by computing $P(G|\mathbf{X})$ from Equation 1 instead of $P(G, \mathbf{K}|\mathbf{X})$ from Equation 5. In other words, we aim to sample over the graph space instead of the joint space of graphs and precision matrices. Direct computation of

the posterior probability $P(G|\mathbf{X})$ for all potential graphs G is feasible just for graphs with less than 10 nodes. This is due to the enormous size of the graph space. We therefore use MCMC-based search algorithms.

3.1 Marginal Pseudo-Likelihood

Bayesian structure learning for GGMs requires to design computationally efficient search algorithms, as we present in Sections 3.2 and 3.3. These type of search algorithms need to compute the Bayes factors of two neighboring graphs

$$\frac{P(G'|\mathbf{X})}{P(G|\mathbf{X})} = \frac{P(\mathbf{X}|G')P(G')}{P(\mathbf{X}|G)P(G)}, \quad (7)$$

where graphs $G = (V, E)$ and G' differ by a single edge $e = (i, j)$, that is $G' = (V, E \cup e)$ or $G' = (V, E \setminus e)$. To compute $P(G|\mathbf{X})$, we need to calculate the marginal likelihood $P(\mathbf{X}|G)$ in Equation 3, which does not have a closed form expression. Thus, we calculate $P(\mathbf{X}|G)$ by utilizing the MPL approach

$$P(\mathbf{X}|G) \approx \tilde{P}(\mathbf{X}|G) = \prod_{h=1}^p P(\mathbf{X}_h|\mathbf{X}_{nb(h)}, G), \quad (8)$$

where $nb(h)$ refers to the neighbors of node h and $\mathbf{X}_{nb(h)}$ is the sub-matrix obtained by selecting the columns in \mathbf{X} corresponding to the nodes/variables that are in $nb(h)$. We then have

$$\begin{aligned} \frac{P(\mathbf{X}|G')}{P(\mathbf{X}|G)} &\approx \frac{\prod_{h=1}^p P(\mathbf{X}_h|\mathbf{X}_{nb(h)}, G')}{\prod_{h=1}^p P(\mathbf{X}_h|\mathbf{X}_{nb(h)}, G)} \\ &= \frac{P(\mathbf{X}_i|\mathbf{X}_{nb(i)}, G')P(\mathbf{X}_j|\mathbf{X}_{nb(j)}, G')}{P(\mathbf{X}_i|\mathbf{X}_{nb(i)}, G)P(\mathbf{X}_j|\mathbf{X}_{nb(j)}, G)}. \end{aligned} \quad (9)$$

For the last step, we use the fact that the graphs G and G' are the same except that one edge $e = (i, j)$ is added or removed while moving from G to G' . As a result, the probabilities of all nodes except X_i and X_j are the same and can be removed from the fraction.

The fractional pseudo-likelihoods in Equation 9 can be expressed in a closed-form by considering a non-informative fractional prior on \mathbf{K} as $W_p(p, \mathbf{U}/n)$, where $W_p(a, \mathbf{A})$ represents a Wishart distribution with an expected value of $a\mathbf{A}^{-1}$. In this case, the local fractional pseudo-likelihood for the node h can be represented as

$$P(\mathbf{X}_h|\mathbf{X}_{nb(h)}, G) = \pi^{-\frac{n-1}{2}} \frac{\Gamma(\frac{n+p_h}{2})}{\Gamma(\frac{p_h+1}{2})} n^{-\frac{2p_h+1}{2}} \left(\frac{|\mathbf{U}_{nb(h) \cup h}|}{|\mathbf{U}_{nb(h)}|} \right)^{-\frac{n-1}{2}}, \quad (10)$$

where p_h is the size of the set $nb(h)$, $\mathbf{U} = \mathbf{X}^T \mathbf{X}$, $\mathbf{U}_{\mathbf{A}}$ denotes the sub-matrix of \mathbf{U} corresponding to the variables in set \mathbf{A} , and matrices $\mathbf{U}_{nb(h)}$ and $\mathbf{U}_{nb(h) \cup h}$ should be positive definite for every h , which is the case if $n \geq \max\{p_h + 1 | h = 1, \dots, p\}$. For more details, see Consonni and Rocca (2012) and Leppä-aho et al. (2017).

Using the outcome from Equation 10 to determine the probabilities in Equation 9's right-hand side allows us to compute the Bayes factor in Equation 7. This computation

involves only four fractional marginal likelihoods. From an optimization perspective, this equation emerges as a favorable choice for MCMC-based search algorithms. In subsequent sections, we introduce two search algorithms leveraging this computational approach. In Section 4, we provide the theoretical justifications for using the MPL approximation within our structure learning search algorithms.

3.2 Birth-Death MCMC Algorithm

The birth-death algorithm, based on a continuous-time Markov process (Preston, 1976), was applied to GGMs by Mohammadi and Wit (2015) to explore the joint space of graphs and precision matrices to approximate $P(G, \mathbf{K} | \mathbf{X})$. Using the MPL approximation, our birth-death MCMC search algorithm (BD-MPL) samples only over the graph space \mathcal{G}_p . During each iteration $s \in \{1, \dots, S\}$, the state of the Markov chain is a certain graph $G^{(s)}$, and it transitions to a new state $G^{(s+1)}$ by adding or removing one edge. These events of adding or removing an edge are called birth and death processes and are modeled as independent Poisson processes. Each edge is added or removed independently of other edges with a Poisson process rate $R_e(G)$. If the birth of an edge $e = (i, j)$ occurs, the process jumps to $G^{+e} = (V, E \cup e)$. If the death of an edge e occurs, the process jumps to $G^{-e} = (V, E \setminus e)$. Since the birth and death processes are modeled as independent Poisson processes, the time between two consecutive events is exponentially distributed with a mean

$$W(G) = \frac{1}{\sum_e R_e(G)}, \quad (11)$$

where the summation is over all $e \in \{(i, j) | 1 \leq i < j \leq p\}$ and $W(G)$ is called the waiting time. The associated birth/death probabilities are

$$P(\text{birth/death of edge } e) = R_e(G)W(G) \text{ for all } e \in \{(i, j) | 1 \leq i < j \leq p\}. \quad (12)$$

The birth-death MCMC search algorithm converges to the target posterior distribution $P(G | \mathbf{X})$ in Equation 1 by considering the following (birth/death) rates

$$R_e(G) = \min \left\{ \frac{P(G' | \mathbf{X})}{P(G | \mathbf{X})}, 1 \right\} \text{ for each } e \in \{(i, j) | 1 \leq i < j \leq p\}, \quad (13)$$

where G' is either G^{+e} or G^{-e} . See Dobra and Mohammadi (2018, Theorem 5.1) for more details. This birth-death algorithm, which searches over the graph space only, is denoted by BD-MPL and Algorithm 1 represents the pseudo-code for this algorithm.

Algorithm 1: BD-MPL search algorithm

Input: Data \mathbf{X} and an initial graph $G = (V, E)$.

- 1 Calculate in parallel the marginal pseudo-likelihood of each node by Equation 10;
- 2 Calculate in parallel all the birth and death rates for each edge by Equation 13;
- 3 **for** S iterations **do**
- 4 **for** *the rates that need to be re-evaluated* **do**
- 5 | Calculate in parallel the birth and death rates by Equation 13;
- 6 **end**
- 7 Calculate the waiting time by Equation 11;
- 8 Update the graph by the birth/death probabilities in Equation 12;
- 9 Update the marginal pseudo-likelihood of the two nodes associated with the flipped edge;
- 10 **end**

Output: Samples from the posterior distribution (1).

Algorithm 1 offers a distinctive computational advantage, particularly in determining birth and death rates, which are ideally suited for parallel execution. Its efficiency is further enhanced by strategic caching techniques. By retaining the marginal pseudo-likelihood of the current graph node, recalculations are only necessary for the two nodes associated with the flipped edge. Importantly, the majority of the rates remain unchanged between successive iterations, which is why we initially calculate all the rates outside the main loop in line 2. By retaining rates from one iteration to the next, only a fraction of these rates require re-evaluation. For a graph with p nodes, only $2p - 3$ of the possible $p(p - 1)/2$ rates need re-assessment. For instance, for a graph with $p = 100$ nodes, the BD-MPL algorithm needs to calculate just 197 rates per iteration, a significant reduction from the 4950 rates requiring updates in the traditional birth-death MCMC algorithm. By incorporating these computational optimizations, we have implemented Algorithm 1 in C++ and ported it to R. This implementation is available within the R package `BDgraph` (Mohammadi et al., 2022) as the `bdgraph.mpl()` function.

The output of Algorithm 1 consists of a set of S sampled graphs $\{G^{(1)}, \dots, G^{(S)}\}$ along with a set of S corresponding waiting times $\{W^{(1)}, \dots, W^{(S)}\}$. The output is the sample of the posterior graph space which allows us to assess the model uncertainty by using Bayesian model averaging. Based on the Rao-Blackwellized estimator given by Cappé et al. (2003), the estimated posterior probability of each graph is proportional to the expectation of the waiting time of that graph (Mohammadi and Wit, 2015). Consequently, the posterior probability of an edge $e = (i, j)$ can be estimated by

$$\hat{P}_e = \frac{\sum_{s=1}^S \mathbf{1}(e \in G^{(s)}) W^{(s)}}{\sum_{s=1}^S W^{(s)}}, \quad (14)$$

which is referred to as the estimated edge-inclusion probability, is suitable for uncertainty quantification as it averages over uncertainty. Within the framework of Bayesian model averaging, these estimated edge-inclusion probabilities offer an insightful summary of the search algorithms across the explored graph space, highlighting the relative importance of all edges. They are commonly used for graph selection with a threshold $0 < v < 1$. A typical threshold is $v = 0.5$, which leads to the estimated graph $\hat{G} = (V, \hat{E})$ where

$\hat{E} = \{e = (i, j) \mid \hat{P}_e \geq 0.5\}$. This approach is analogous to the median-probability model of Barbieri and Berger (2004) and is employed in our simulation study in Section 5 to report F1 scores. For practical graph estimation, we recommend using this median-probability approach, as suggested by Barbieri and Berger (2004), rather than the model with the highest posterior probability.

3.3 Reversible Jump MCMC Algorithm

To sample from $P(G|\mathbf{X})$ as shown in Equation 1, we utilize a reversible jump MCMC search algorithm (Green, 1995). In each iteration, the algorithm proposes a new graph G' by either adding or deleting an edge from the existing graph G . The proposed graph G' is accepted with the acceptance probability defined as

$$\alpha(G, G') = \min \left\{ \frac{P(G'|\mathbf{X})q(G'|G)}{P(G|\mathbf{X})q(G|G')}, 1 \right\}, \quad (15)$$

where $q(G'|G)$ is the probability that given the current graph G , the graph G' is proposed by adding or deleting one edge from G . Adopting a uniform distribution as the proposal distribution over the neighboring state, we have $q(G|G') = q(G'|G) = 1/nb_{max}$, where $nb_{max} = p(p-1)/2$ that is the maximum number of neighboring graphs that diverge from graph G by a single edge. With this consideration, $\alpha(G, G')$ aligns with $R_e(G)$ as expressed in Equation 13. It highlights the similarity between the reversible jump MCMC algorithm and the birth-death MCMC. For more details, see Cappé et al. (2003).

One limitation of using a uniform proposal is that the probability of removing an edge equals $|E|/nb_{max}$ which usually tends to be low. Addressing this, Dobra et al. (2011) introduced a two-step approach. First, an edge is added or removed with a probability 0.5. Second, an edge is randomly selected from the relevant subset. Following this idea, the proposal distribution can be described as

$$q(G|G') = \begin{cases} \frac{1}{2|E|}, & \text{for all } e \in E, \\ \frac{1}{2|\bar{E}|}, & \text{for all } e \in \bar{E}, \\ \frac{1}{nb_{max}}, & \text{when } |E| \text{ or } |\bar{E}| \text{ is } 0, \end{cases}$$

where $e = (i, j)$ refers to the edge under consideration for inclusion or exclusion from graph G . Taking a step forward, van den Boom et al. (2022) introduced an optimized proposal technique for graphs. This method derives insights from the target distribution, leveraging the principles of locally balanced proposals as discussed by Zanella (2020). Further details can be explored in van den Boom et al. (2022, Section 2.3).

Our reversible jump MCMC search algorithm is abbreviated to RJ-MPL and the pseudo-code for this algorithm is described in Algorithm 2. Similar to Algorithm 1, we implement this algorithm in C++ and ported it to R. It is available within the R package `BDgraph` (Mohammadi et al., 2022) as `bdgraph.mpl()` function.

Algorithm 2: RJ-MPL search algorithm

Input: Data \mathbf{X} and an initial graph $G = (V, E)$.

- 1 Calculate in parallel the marginal pseudo-likelihood of each node by Equation 10;
- 2 **for** S iterations **do**
- 3 Draw a proposal graph by selecting an edge to flip;
- 4 Calculate the acceptance probability by Equation 15 and update the graph;
- 5 Update the marginal pseudo-likelihood for the pair of nodes associated with the flipped edge;
- 6 **end**

Output: Samples from the posterior distribution (1).

The output of Algorithm 2 consists of a set of S sampled graphs $\{G^{(1)}, \dots, G^{(S)}\}$ over the posterior graph space. This sample for the RJ-MPL approach can be used to calculate the estimated edge-inclusion probabilities (\hat{P}_e) using Equation 14 with $W^{(s)} = 1$ for $s \in \{1, \dots, S\}$. Similar to the BD-MPL approach in Section 3.2, \hat{P}_e can be used to assess model uncertainty and for model selection.

3.4 Estimation for Precision Matrix

The BD-MPL and RJ-MPL algorithms are designed to recover the underlying graph structure from the data. In practice, it is often important to estimate the precision matrix as well. Here, we demonstrate how to estimate the true precision matrix using the graph samples obtained from the BD-MPL and RJ-MPL algorithms. We present two approaches for achieving this.

One approach is to first estimate the graph structure using the edge inclusion probabilities (14) derived from the BD-MPL or RJ-MPL algorithms. Specifically, we can obtain the estimated graph $\hat{G} = (V, \hat{E})$ where $\hat{E} = \{e = (i, j) \mid \hat{P}_e \geq 0.5\}$, and \hat{P}_e represents the estimated edge-inclusion probabilities in Equation 14. This estimated graph can then be used to sample from the precision matrix using the G -Wishart distribution, as defined in Equation 4, where $\mathbf{K} \mid \hat{G} \sim W_{\hat{G}}(b+n, \mathbf{D} + \mathbf{U})$, representing the posterior distribution of the precision matrix.¹ The mean of this set of samples will be the estimated precision matrix. It is important to note that the estimated precision matrix will be positive definite, as the output of the Lenkoski (2013) algorithm ensures positive definiteness.

Another approach is to use the sampled graphs $\{G^{(1)}, \dots, G^{(S)}\}$ generated by the BD-MPL or RJ-MPL algorithms, and then sample the corresponding precision matrices $\{\mathbf{K}^{(1)}, \dots, \mathbf{K}^{(S)}\}$ from $W_G(b+n, \mathbf{D} + \mathbf{U})$ using the Lenkoski (2013) algorithm, similar to the first approach. However, this method may not be feasible for very large-scale graphs, as saving all the sampled graphs can lead to memory issues. See, for example, Mohammadi and Wit (2019, Appendix).

¹This step can be performed using the sampling algorithm developed by Lenkoski (2013), which is implemented in the R package `BDgraph`, specifically through the `rgwish()` function.

4 Theoretical Properties

In this section, we establish the theoretical properties of the BD-MPL and RJ-MPL algorithms (Algorithms 1 and 2), including convergence proofs and sparsity selection consistency. Let \hat{G} be the estimate of the true graph G^* , obtained by thresholding the estimated edge-inclusion probabilities (14) at some threshold $0 < v < 1$, where $\hat{G} = (V, \hat{E})$ with $\hat{E} = \{e = (i, j) \mid \hat{P}_e \geq v\}$. We aim to prove that \hat{G} converges in probability to the true graph G^* as both the number of observations n and the number of MCMC iterations S approach infinity. First, we demonstrate in the following lemma that the BD-MPL and RJ-MPL algorithms converge to the pseudo-posterior distribution $\tilde{P}(G|\mathbf{X})$, our target posterior distribution (1), by utilizing the MPL approach from Equation 8. Subsequently, in Lemma 2, we show that the pseudo-posterior distribution concentrates around the true graph G^* .

Lemma 1 (Convergence). *Let $\{G^{(1)}, \dots, G^{(S)}\}$ be the Markov chain generated by either the BD-MPL or RJ-MPL algorithm. As the number of iterations S approaches infinity, these Markov chains converge to the target pseudo-posterior distribution $\tilde{P}(G|\mathbf{X})$. Moreover, the estimated edge-inclusion probability \hat{P}_e , as defined in Equation 14, converges to the true edge-inclusion probability P_e . That is,*

$$\lim_{S \rightarrow \infty} \hat{P}_e = P_e = \sum_{G \in \mathcal{G}_p} \mathbf{1}(e \in G) \tilde{P}(G|\mathbf{X})$$

for all $e \in \{(i, j) \mid 1 \leq i < j \leq p\}$.

Proof. The three conditions necessary for this lemma are irreducibility, aperiodicity, and the balance condition (Tierney, 1994). Although detailed balance is more restrictive than necessary for ensuring ergodicity and the correct limiting distribution, it is a convenient condition to impose in the practical design of samplers (Green, 1995). For Algorithm 1, detailed balance is satisfied by considering the birth/death rates as defined in Equation 13. For more details, see Dobra and Mohammadi (2018, Theorem 5.1). Similarly, these conditions hold for Algorithm 2 by considering the acceptance probability as defined in Equation 15. See, for example, Green (1995). \square

In the following lemma, we establish posterior consistency by demonstrating that the posterior mass assigned to the true sparsity pattern (the true graph G^*) converges to one in probability as the number of observations n approaches infinity.

Lemma 2 (Posterior Contraction). *The mass of the pseudo-posterior $\tilde{P}(G|\mathbf{X})$ assigned to the true graph $G^* = (V, E^*)$ converges to one in probability. That is, as $n \rightarrow \infty$,*

$$\tilde{P}(G^*|\mathbf{X}) \rightarrow 1$$

in probability.

Proof. Based on Equations (1) and (8), we have

$$\tilde{P}(G^*|\mathbf{X}) \propto P(G^*) \prod_{j=1}^p P(\mathbf{X}_j | \mathbf{X}_{nb^*(j)}, G^*),$$

where $nb^*(j)$ denotes the set of neighbors (or Markov blanket) of node j . These neighbors uniquely define the true graph G^* for $j \in \{1, \dots, p\}$, and these are the only parts of $\tilde{P}(G^*|\mathbf{X})$ that depend on n . Now, considering an arbitrary graph G' (not equal to G^*) with corresponding neighbors $nb'(j)$ of node $j \in \{1, \dots, p\}$, we have

$$\frac{\tilde{P}(G^*|\mathbf{X})}{\tilde{P}(G'|\mathbf{X})} = \frac{P(G^*)}{P(G')} \times \prod_{j=1}^p \frac{P(\mathbf{X}_j|\mathbf{X}_{nb^*(j)}, G^*)}{P(\mathbf{X}_j|\mathbf{X}_{nb'(j)}, G')}.$$

For all $j \in \{1, \dots, p\}$, as $n \rightarrow \infty$, we can derive

$$\log \left(\frac{P(\mathbf{X}_j|\mathbf{X}_{nb^*(j)}, G^*)}{P(\mathbf{X}_j|\mathbf{X}_{nb'(j)}, G')} \right) \rightarrow \infty$$

in probability; this result follows directly from Leppä-aho et al. (2017, Theorem 2, Lemma 1, and 2). Essentially, this means that by using the marginal pseudo-likelihood function in Equation 8, the true neighbors $nb^*(j)$ are preferred over any other set $nb'(j)$ as the number of observations n approaches infinity. Considering this, as $n \rightarrow \infty$,

$$\frac{\tilde{P}(G^*|\mathbf{X})}{\tilde{P}(G'|\mathbf{X})} \rightarrow \infty$$

in probability. The convergence then follows. \square

The consistency of model selection criteria is a significant asymptotic property. Under the assumption that the generating distribution adheres to a Markov network structure, consistency in model selection means that the BD-MPL or RJ-MPL algorithms will favor the true graph as the sample size approaches infinity. In the following theorem, we establish the main result regarding posterior consistency. Specifically, we demonstrate that the estimated graph \hat{G} , derived from the estimated edge-inclusion probabilities (14) and the output of the BD-MPL or RJ-MPL algorithms, converges to the true graph G^* as the sample size n tends to infinity.

Theorem 1 (Selection Consistency). *Let \hat{P}_e denote the estimated edge-inclusion probabilities (14) obtained by either the BD-MPL or RJ-MPL algorithm for S iterations. Let \hat{G} be the estimate of the true graph G^* obtained by thresholding these edge-inclusion probabilities at some threshold $0 < v < 1$. Then, as $n \rightarrow \infty$ and $S \rightarrow \infty$,*

$$P(\hat{G} = G^*) \rightarrow 1$$

in probability.

Proof. Due to Lemma 1, for all $e \in \{(i, j) | 1 \leq i < j \leq p\}$, we have

$$\lim_{S \rightarrow \infty} \hat{P}_e = P_e = \sum_{G \in \mathcal{G}_p} \mathbf{1}(e \in G) \tilde{P}(G|\mathbf{X}).$$

Notice that we have $P_e \geq \tilde{P}(G^*|\mathbf{X})$ for all $e \in G^*$ and $P_e \leq 1 - \tilde{P}(G^*|\mathbf{X})$ for all $e \notin G^*$. Then,

$$\begin{aligned} P(\hat{G} = G^*) &= P(P_e \geq v \quad \forall e \in G^* \text{ and } P_e < v \quad \forall e \notin G^*) \\ &\geq P\left(\tilde{P}(G^*|\mathbf{X}) \geq v \text{ and } 1 - \tilde{P}(G^*|\mathbf{X}) < v\right) \\ &= P\left(\tilde{P}(G^*|\mathbf{X}) \geq \max(v, 1 - v)\right). \end{aligned}$$

The result follows from Lemma 2. \square

The theoretical properties presented in this section validate the concept of MPL for the BD-MPL and RJ-MPL algorithms as the number of observations tends to infinity. However, it is also crucial to examine the practical performance of these algorithms when dealing with a limited number of observations. In the following section, we conduct extensive numerical simulations to evaluate the performance of our algorithms compared to state-of-the-art methods.

5 Simulation Study

In this simulation study, we assess the accuracy and computational efficiency of our proposed graph recovery algorithms: the birth-death and the reversible jump MCMC search algorithms enhanced with MPL estimation. These algorithms are respectively referred to as BD-MPL (outlined in Algorithm 1) and RJ-MPL (outlined in Algorithm 2). To gain a comprehensive understanding, we compare the results with three state-of-the-art Bayesian approaches. The first is the birth-death MCMC algorithm (BD) introduced by Mohammadi and Wit (2015) and Mohammadi et al. (2023). The second is a method established by Wang (2015) (SS), which employs a block Gibbs sampler based on the spike-and-slab prior distribution. The third is the B-CONCORD approach developed by Jalali et al. (2020), which uses a generalized likelihood function together with a spike-and-slab prior distribution. The code for reproducing the results in this section is available on a publicly accessible GitHub page². All computations were performed on the University of Amsterdam’s super-computer (Snellius system) using one core on a Lenovo® ThinkSystem SR645 2.60 GHz Processor. The simulation parameters are detailed in Section 5.1, the performance metrics are discussed in Section 5.2, and the findings are presented in Section 5.3.

5.1 Simulation Settings

We outline the settings used for the simulation study, including small- ($p = 10$), medium- ($p = 100$), and large-scale graphs ($p = 1000$). Three types of graphs are examined:

1. **Random:** Graphs where a number of edges are randomly sampled without replacement.
2. **Cluster:** Graphs with two clusters (when $p \in \{10, 100\}$) and eight clusters (when $p = 1000$), where each cluster mirrors the structure of the **Random** graph.
3. **Scale-free:** Spanning trees generated using the B-A algorithm introduced by Albert and Barabási (2002).

For both **Random** and **Cluster** graphs, we explore both ‘*sparse*’ and ‘*dense*’ variants. To accurately represent *sparse* and *dense* graphs in practice, we determine the number of edges n_e using the formula $\max(ap, bp(p-1)/2)$, where $a = 0.5$ and $b = 0.5\%$ for sparse graphs, and $a = 2$ and $b = 5\%$ for dense graphs. The edge density for each graph type and each value of p is presented in Table 1.

In most GGM literature, the number of observations n is chosen using one of two approaches: either keeping n fixed as p increases (e.g., Sagar et al. 2024), or setting n as

²<https://github.com/lucasvogels33/Large-scale-BSL-for-GGMs-using-MPL>

p	10		100		1000	
	Sparse	Dense	Sparse	Dense	Sparse	Dense
Density						
Random	11.1%	44.4%	1.0%	5.0%	0.5%	5.0%
Cluster	11.1%	44.4%	1.0%	5.0%	0.5%	5.0%
Scale-free	20.0%		2.0%		0.2%	

Table 1: *The edge density of the graphs is defined as the proportion of the number of edges to the total number of possible edges in the graphs.*

a multiple of p (e.g., Jalali et al. 2020). Here, we consider a logarithmic relation between n and p , as suggested by posterior contraction rates (Sagar et al., 2024, Theorem 4.6) and convergence bounds for the graphical lasso algorithm (Rothman et al., 2008, Theorem 2). Consequently, we select $n = 20 \log(p)$ for a 'low' number of observations and $n = 350 \log(p)$ for a 'high' number of observations. An exception is made for $p = 1000$, where $n = 20 \log(p) = 60$ was too low for all algorithms to provide meaningful results. In this case, we chose $n = 400$.

In each simulated graph G , the precision matrix \mathbf{K} was generated from the G -Wishart distribution $W_G(3, \mathbf{I}_p)$. For p in $\{10, 100\}$, we generated 16 graphs along with their corresponding precision matrices, while for $p = 1000$, we obtained 8 such pairs. Subsequently, for each pair G and \mathbf{K} , we sampled n data points from the p -dimensional Gaussian distribution $\mathcal{N}_p(\mathbf{0}, \mathbf{\Sigma})$ with mean zero and covariance matrix $\mathbf{\Sigma} = \mathbf{K}^{-1}$. The data was generated using the `bdgraph.sim()` function from the R package `BDgraph` (Mohammadi et al., 2022).

To ensure comparable computing times, all algorithms were coded in C++ and then ported to R, utilizing the same routines wherever feasible. Following the approach of Wang (2015), the hyperparameters for the SS method were chosen as $\epsilon = 0.02$, $v = 2$, and $\lambda = 1$. For the prior distribution of the graph G , as defined in Equation 2, we set $\beta = 0.2$, except for the B-CONCORD method for which $\beta = 0.5$. Each MCMC run started with an empty graph with p nodes, except for the B-CONCORD method, which started with a full graph. These choices for the B-CONCORD method were due to the package provided by the authors (Jalali et al., 2020) not allowing for the specification of the initial graph and the value of β , so we decided to maintain the authors' original setup. The number of iterations varied per instance, as detailed in Table 13 in the Appendix. The BD-MPL and RJ-MPL methods were implemented using the `BDgraph` R package (Mohammadi et al., 2022), while the SS method utilized the `ssgraph` R package (Mohammadi, 2022). For the B-CONCORD method, we used the software package provided by the authors (Jalali et al., 2020).

5.2 Performance Metrics

The methods will be evaluated based on the accuracy of the graph recovery and the computational cost. To evaluate the accuracy of graph recovery, we utilize the MCMC sampled graphs $\{G^{(1)}, \dots, G^{(S)}\}$, where S represents the number of MCMC iterations, to calculate the edge inclusion probabilities as defined by Equation 14. Subsequently, we compute five accuracy metrics introduced below.

The Area Under the Receiver Operating Characteristic Curve (AUC-ROC) (Hanley and McNeil, 1982) evaluates the classifier's ability to distinguish between edges in the true graph

from edges not in the true graph. The ROC curve plots the True Positive Rate against the False Positive Rate at various threshold settings. The AUC-ROC measures the area under the curve and ranges from 0 to 1, with higher values indicating better discriminatory performance.

The Area Under the Precision-Recall Curve (AUC-PR) (Davis and Goadrich, 2006) is useful for evaluating performance on imbalanced data sets, such as sparse graphs in this case. The PR curve plots Precision (the proportion of true positive edges among all predicted edges) against Recall (the proportion of actual edges correctly identified) at various thresholds. The AUC-PR value ranges from 0 to 1, with higher values indicating better performance in identifying edges.

The $F1$ Score (Powers, 2020) is the harmonic mean of Precision and Recall, providing a single metric that balances the two aspects. It is defined as

$$F1 = 2 \times \frac{\text{Precision} \times \text{Recall}}{\text{Precision} + \text{Recall}}. \quad (16)$$

To report the $F1$ values, we first obtain the estimated graph $\hat{G} = (V, \hat{E})$, where $\hat{E} = \{e = (i, j) \mid \hat{P}_e \geq 0.5\}$. In Bayesian graphical learning, the $F1$ Score ranges from 0 to 1, with higher values indicating better overall performance in detecting true edges while minimizing false positives and false negatives. This balance is particularly important when both types of errors have significant implications for the accuracy of the inferred graph.

Pr^+ and Pr^- represent the average inclusion probability for all edges and non-edges, respectively, in the true graph $G = (V, E)$ (Vogels et al., 2023). They are calculated as

$$Pr^+ = \frac{1}{|E|} \sum_{e \in E} \hat{P}_e \quad (17)$$

and

$$Pr^- = \frac{1}{|\bar{E}|} \sum_{e \in \bar{E}} \hat{P}_e, \quad (18)$$

where \hat{P}_e are the estimated edge-inclusion probabilities (14). These two probabilities serve as measures of calibration accuracy. Ideally, the algorithms should achieve a high Pr^+ to enhance edge detection accuracy and a low Pr^- to effectively reject edges that are not present in the true graph $G = (V, E)$.

We assess the computational efficiency of the algorithms by measuring the time required for AUC-PR convergence. Convergence is defined as the point at which the AUC-PR value stabilizes, specifically when it is within 0.01 of its final iteration value.

5.3 Results

We begin by evaluating the computational efficiency of the algorithms, as shown by the computational time required for AUC-PR convergence in Table 2. For AUC-ROC convergence, we refer to Table 8 in the Supplementary Material. For $p = 10$, the computational costs of the algorithms are comparable, with all converging in less than a second. For $p = 100$, the RJ-MPL, BD-MPL, SS, and B-CONCORD algorithms converge within seconds to minutes, whereas the BD method requires hours. For $p = 1000$, the BD algorithms do not converge

within five days. In contrast, the BD-MPL, RJ-MPL, SS, and B-CONCORD algorithms converge within hours to days, with BD-MPL being up to ten times faster than RJ-MPL, SS, and B-CONCORD.

p	Graph	Density	n	RJ-MPL	BD-MPL	BD	SS	B-CONCORD	
1000	Random	Sparse	400	2494	41	-	531	972	
		Sparse	1050	1998	96	-	543	418	
		Dense	400	2706	350	-	3012	3731	
		Dense	1050	2434	1065	-	3297	2099	
	Cluster	Sparse	400	2212	33	-	436	975	
		Sparse	1050	1794	74	-	489	615	
		Dense	400	2509	283	-	2386	3681	
		Dense	1050	3003	396	-	2654	1711	
	Scale-free	Sparse	400	4104	43	-	339	1808	
		Sparse	1050	4053	144	-	1281	1508	
	100	Random	Sparse	40	6	2	103	0	7
			Sparse	700	0	0	34	2	3
Dense			40	2	0	101	0	5	
Dense			700	2	0	72	1	3	
Cluster		sparse	40	6	3	86	1	6	
		Sparse	700	1	1	45	1	4	
		Dense	40	0	0	115	0	4	
		Dense	700	1	0	78	1	1	
Scale-free		Sparse	40	2	1	103	0	5	
		Sparse	700	2	1	67	1	4	
10		Random	Sparse	20	0	0	0	0	0
			Sparse	20	0	0	0	0	0
	Sparse		350	0	0	0	0	0	
	Dense		20	0	0	0	0	0	
	Dense		350	0	0	0	0	0	
	Cluster	Sparse	20	0	0	0	0	0	
		Sparse	350	0	0	0	0	0	
		Dense	20	0	0	0	0	0	
		Dense	350	0	0	0	0	0	
	Scale-free	Sparse	20	0	0	0	0	0	
		Sparse	350	0	0	0	0	0	

Table 2: Computational cost (T) in minutes until AUC-PR convergence for different instances. T represents the average time until AUC-PR convergence, based on 16 replications for $p \in \{10, 100\}$ and 8 replications for $p = 1000$. A “-” indicates that an algorithm did not converge within five days. The best methods are highlighted in bold.

Table 3 presents the AUC-PR scores of the methods. For small ($p = 10$) and medium ($p = 100$) graphs, the AUC-PR values are similar across methods, with the BD approaches showing slightly higher values. However, for large problems ($p = 1000$), the AUC-PR values vary significantly. The commonly used BD method yields AUC-PR values around zero, indicating its inefficacy for large-scale problems within a reasonable timeframe (five days in this study). In scenarios with large problems ($p = 1000$), the RJ-MPL and BD-MPL methods achieve the highest AUC-PR results, followed by SS, B-CONCORD, and finally BD. Tables 2 and 3 indicate that for large-scale graphs ($p = 1000$), the BD-MPL algorithm performs the best in terms of both computational time and accuracy.

We report the results for the remaining graph recovery precision metrics in the Supplementary Material: AUC-ROC in Table 9, $F1$ in Table 10, Pr^+ in Table 11, and Pr^- in Table 12. For AUC-ROC and $F1$, the RJ-MPL and BD-MPL methods perform as well as or better than the other algorithms. For Pr^+ at $p = 100$ and $p = 1000$ (Table 11), B-CONCORD occasionally shows higher values, likely due to its higher Pr^- values. It is worth noting that, in general, our MPL approaches (RJ-MPL and BD-MPL) perform well in terms of AUC-PR, $F1$, and Pr^- , but not as well for Pr^+ . This tendency is likely because our approaches tend to select sparser graphs overall compared to other approaches. Ideally, we aim for a high Pr^+ to improve edge detection accuracy while maintaining a low Pr^- to effectively reject non-edges.

Figure 2 presents the graph precision recovery metrics over time, specifically AUC-PR (top row) and $F1$ (bottom row) scores (see Figure 7 in the supplementary material for AUC-ROC, Pr^+ , and Pr^- metrics). The left column displays metrics for medium-scale graphs ($p = 100$, $n = 700$, *sparse Cluster* graph), while the right column displays metrics for large-scale graphs ($p = 1000$, $n = 1050$, *dense Cluster* graph). For the medium-scale problem, all methods except BD converge quickly, with BD showing relatively low Pr^+ and high Pr^- values. For the large-scale problem, the BD-MPL method’s graph recovery precision metrics converge significantly faster than those of the other methods.

In summary, for *large-scale* problems (graphs with $p = 1000$), the BD-MPL and RJ-MPL approaches achieve significantly lower computational costs while maintaining high accuracy compared to state-of-the-art methods. Additionally, BD-MPL has several advantages over RJ-MPL, as it converges faster (as indicated in Figure 2) and its computationally intensive parts can be implemented in parallel, as discussed in Section 3.2. Therefore, BD-MPL and RJ-MPL are better suited for large-scale problems, such as graphs with $p = 1000$ or more. For *medium-scale* problems (graphs with around 100 nodes), both BD and BD-MPL methods demonstrate similar and higher accuracy than other methods (Table 3). For these cases, the computational cost for the BD algorithm ranges between one to two hours, while for the BD-MPL algorithm, it is at most three minutes (Table 2). For *small-scale* problems (graphs with $p = 10$), the BD method shows slightly higher accuracy in most cases compared to the BD-MPL method. Generally, we recommend using the BD or SS methods for small-scale problems (graphs with around 10 nodes).

p	Graph	Density	n	RJ-MPL	BD-MPL	BD	SS	B-CONCORD	
1000	Random	Sparse	400	0.67	0.70	0.01	0.66	0.66	
		Sparse	1050	0.79	0.81	0.00	0.72	0.79	
		Dense	400	0.39	0.43	0.05	0.42	0.31	
		Dense	1050	0.56	0.61	0.05	0.56	0.50	
	Cluster	Sparse	400	0.70	0.72	0.01	0.67	0.68	
		Sparse	1050	0.81	0.83	0.01	0.74	0.78	
		Dense	400	0.55	0.59	0.05	0.55	0.48	
		Dense	1050	0.71	0.74	0.05	0.7	0.58	
	Scale-free	Sparse	400	0.66	0.68	0.00	0.68	0.62	
		Sparse	1050	0.78	0.8	0.00	0.76	0.72	
	100	Random	Sparse	40	0.50	0.50	0.54	0.55	0.50
			Sparse	700	0.89	0.89	0.89	0.84	0.86
Dense			40	0.37	0.37	0.40	0.43	0.38	
Dense			700	0.86	0.86	0.86	0.79	0.82	
Cluster		Sparse	40	0.49	0.49	0.52	0.53	0.49	
		Sparse	700	0.87	0.88	0.88	0.84	0.83	
		Dense	40	0.40	0.39	0.43	0.45	0.41	
		Dense	700	0.87	0.87	0.87	0.80	0.83	
Scale-free	Sparse	40	0.41	0.41	0.47	0.47	0.41		
	Sparse	700	0.87	0.87	0.89	0.82	0.77		
10	Random	Sparse	20	0.52	0.52	0.54	0.52	0.52	
		Sparse	350	0.91	0.91	0.92	0.89	0.89	
		Dense	20	0.68	0.69	0.69	0.68	0.68	
		Dense	350	0.94	0.93	0.93	0.93	0.91	
	Cluster	Sparse	20	0.50	0.50	0.50	0.50	0.48	
		Sparse	350	0.84	0.85	0.85	0.84	0.86	
		Dense	20	0.81	0.81	0.83	0.81	0.77	
		Dense	350	0.95	0.95	0.95	0.94	0.94	
	Scale-free	Sparse	20	0.61	0.61	0.65	0.65	0.60	
		Sparse	350	0.90	0.91	0.91	0.89	0.87	

Table 3: $AUC - PR$ scores of the algorithms for different instances. The $AUC - PR$ reaches its best score at 1 and its worst at 0. The values are averages over 16 replications for $p \in \{10, 100\}$ and over 8 replications for $p = 1000$. The best methods are highlighted in bold.

6 Applications

We apply our proposed BD-MPL and RJ-MPL algorithms to two real-world data sets: a medium-scale data set (with 100 variables) in Subsection 6.1 and a large-scale data set (with 623 variables) in Subsection 6.2. To further demonstrate the capabilities and the

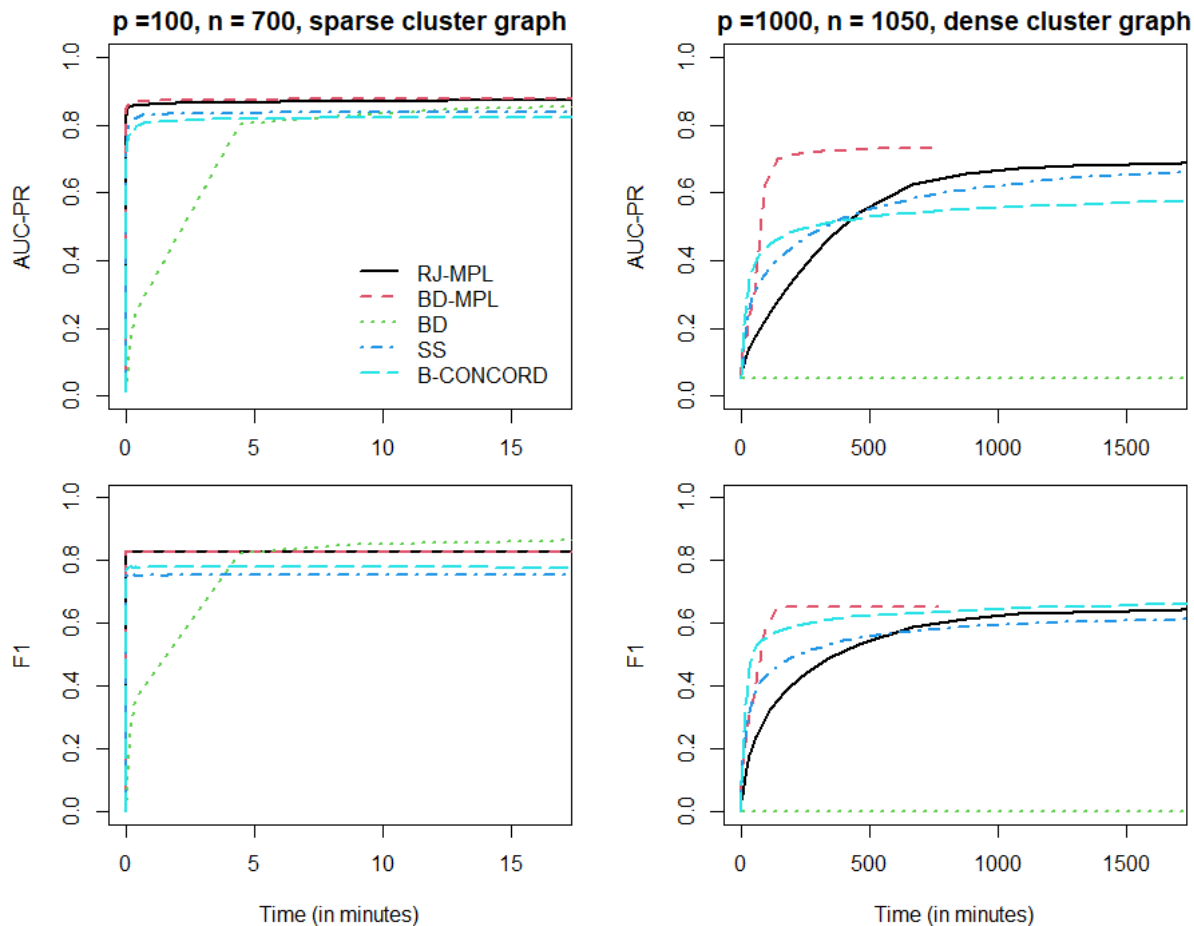


Figure 2: *The convergence of AUC-PR (top row) and F1 (bottom row) scores over running time for all algorithms (RJ-MPL, BD-MPL, BD, SS, B-CONCORD). The plots on the left represent the instance with $p = 100$, $n = 700$ for the sparse Cluster graph. The plots on the right represent the instance with $p = 1000$, $n = 1050$ for the dense Cluster graph.*

performances of the BD-MPL and RJ-MPL algorithms, we compared them with leading Bayesian methods on these data sets.

6.1 Application to Human Gene Expression

Here, we apply the BD-MPL and RJ-MPL algorithms to infer a human gene network. We compare the resulting network with findings from the literature and networks obtained using state-of-the-art Bayesian structure learning methods, namely the BD, SS, and B-CONCORD methods. The data set we utilize contains genetic data for $p = 100$ genes from $n = 60$ unrelated individuals. This data set is available in the `BDgraph` R package (Mohammadi et al., 2022). Detailed information on the collection of this data can be found in Stranger et al. (2007) and Bhadra and Mallick (2013). This data set has also been employed for medium-scale Bayesian structure learning (Mohammadi and Wit, 2015; Li et al., 2019; Mohammadi and Wit, 2019; van den Boom et al., 2022; Vogels et al., 2023).

Genes are specific sequences of DNA that play a critical role in the functioning of organisms. Gene expression is the process through which these genes produce proteins,

which then influence various biological functions. Some proteins have direct effects on the organism, like initiating the breakdown of food. Others serve a regulatory role by “activating” other genes, leading to the production of additional proteins that further activate more genes, creating a cascade of interactions. These activation relationships can be represented in a gene network, where each node corresponds to a gene, and each edge signifies an activation relationship between two genes. Mapping and understanding these gene networks are vital for elucidating disease susceptibility, ultimately contributing to advancements in treatment and public health (Stranger et al., 2007).

In our study, we have a data matrix $\mathbf{X} = (\mathbf{X}^{(1)}, \dots, \mathbf{X}^{(n)})^T$ of dimensions $n \times p$, with elements X_{li} denoting the level of protein corresponding to gene $i \in \{1, \dots, p\}$, measured in individual $l \in \{1, \dots, n\}$. We transformed our non-Gaussian continuous variables X_1, \dots, X_p to Gaussian variables $\mathbf{Z} := (Z_1, \dots, Z_p)$ with mean zero, *i.e.*, $\mathbf{Z} \sim \mathcal{N}_p(\mathbf{0}, \Sigma_Z)$, ensuring that the sparsity of $\mathbf{K}_Z = \Sigma_Z^{-1}$ still encodes the conditional dependencies among the variables. Specifically, we used a transformation based on cumulative distribution functions (Liu et al., 2009) included in the `bdgraph.npn()` function in the `BDgraph` R package (Mohammadi et al., 2022).

The number of MCMC iterations is set to 30 million for RJ-MPL, one million for BD-MPL, 100,000 for BD, 20,000 for SS, and 200,000 for B-CONCORD, with half of the iterations considered burn-in. Simulated experiments in Section 5 on $p = 100$ graphs confirmed that these values are sufficient for MCMC convergence. The initial parameter settings for running the algorithms were the same as those in the simulation study in Section 5.1.

Figure 3 illustrates the number of edges in the Markov chain for each algorithm over running time. It is important to note that the number of edges in each MCMC iteration does not indicate the number of edges in the final graph. The results show that the BD-MPL algorithm converges the fastest (in 5 minutes), followed by the B-CONCORD (in 7 minutes) and RJ-MPL (in 10 minutes) algorithms. The SS and BD algorithms converge the slowest, taking over 17 minutes.

Figure 4 displays the gene networks inferred by each algorithm, showing only edges with inclusion probabilities (14) greater than 0.9. All five algorithms identify similar tree structures, corroborating findings from earlier research. For instance, the trees spanning the nodes $\{38, 13, 10, 16, 18, 8, 4\}$ correspond to the trees shown in Bhadra and Mallick (2013, Figure 4).

Subsequently, we evaluate the results using two metrics: the average absolute differences in edge inclusion probabilities for all unique edges, as shown in Table 4, and the percentage of edges identified by method A that are also detected by method B, using a threshold of 0.9 for edge inclusion probability, as presented in Table 5. The average absolute differences in edge inclusion probabilities in Table 4 are relatively low. However, these differences are influenced by the presence of many edges with inclusion probabilities close to zero.

Table 5 demonstrates that, with a 0.9 threshold for edge inclusion probabilities, B-CONCORD identifies the highest number of edges (87), followed by RJ-MPL and BD-MPL (75 and 73, respectively), BD (68), and SS (35). Starting with SS, which identifies the fewest edges, Table 5 shows that nearly all edges identified by SS are also identified by the other algorithms. For BD, 68% to 79% of its identified edges overlap with those identified by other algorithms, such as B-CONCORD, RJ-MPL, and BD-MPL, which have a higher number of identified edges. Notably, B-CONCORD, BD-MPL, and RJ-MPL

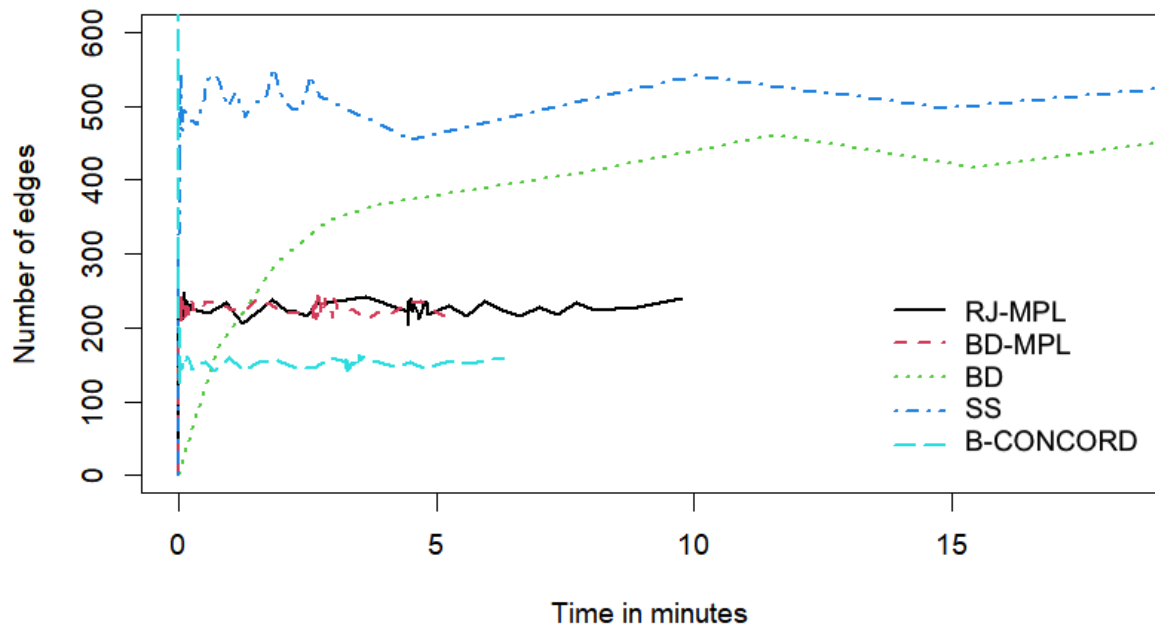


Figure 3: Plot tracking the number of edges in the Markov chain state over running time for each algorithm on the human gene dataset to check convergence.

	BD-MPL	RJ-MPL	BD	SS	B-CONCORD
BD-MPL	-	0.005	0.067	0.077	0.023
RJ-MPL	-	-	0.067	0.077	0.023
BD	-	-	-	0.045	0.074
SS	-	-	-	-	0.085
B-CONCORD	-	-	-	-	-

Table 4: Average absolute difference in edge inclusion probabilities between algorithms on the human gene data set.

exhibit substantial overlap: approximately 71% to 75% of B-CONCORD’s edges are also identified by BD-MPL and RJ-MPL, respectively, while 97% of BD-MPL’s edges overlap with those identified by RJ-MPL.

6.2 Application to Gene Expression in Immune Cells

We evaluate the performance and applicability of our proposed algorithms (BD-MPL and RJ-MPL) by comparing them with leading Bayesian methods (BD, SS, and B-CONCORD) on a large-scale gene network using the GSE15907 microarray dataset from Painter et al. (2011) and Desch et al. (2011). This dataset comprises gene expression data from 24,922 genes in 653 mouse immune cells, obtained from the Immunological Genome Project (Heng et al., 2008), and previously analyzed by Chandra et al. (2021) using Bayesian structure

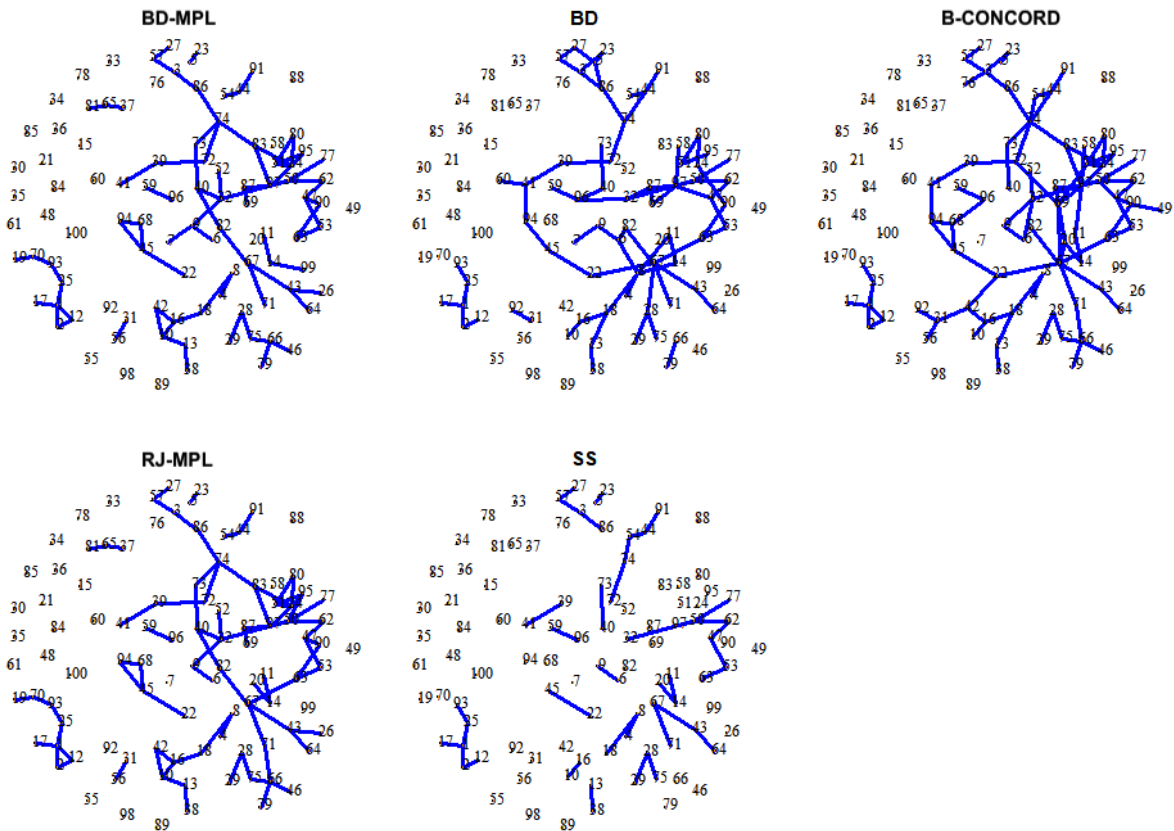


Figure 4: *Estimated graphs based on the BD-MPL, RJ-MPL, BD, SS, and B-CONCORD algorithms for the human gene data set. Only edges with inclusion probabilities greater than 0.9 are displayed.*

	BD-MPL	RJ-MPL	BD	SS	B-CONCORD
BD-MPL (73)	-	0.97	0.63	0.45	0.85
RJ-MPL (75)	0.95	-	0.61	0.45	0.87
BD (68)	0.68	0.68	-	0.49	0.79
SS (35)	0.94	0.97	0.94	-	1.00
B-CONCORD (87)	0.71	0.75	0.62	0.40	-

Table 5: *Proportion of edges identified by the row algorithm that are also found by the column algorithm on the human gene data set, using an edge inclusion probability threshold of 0.9. The numbers in brackets indicate the count of edges with an edge inclusion probability greater than 0.9.*

learning methods.

The immune system defends organisms from diseases through lymphocytes (T cells, B cells, NK cells), neutrophils, and monocytes/macrophages. Genes within these cells produce proteins, some directly impacting disease response, while others initiate cascades by activating additional genes. These activation relationships are represented in gene networks, where nodes signify genes and edges denote activation connections. Exploring these

networks is crucial for advancing immune system understanding and treatment strategies.

Following Chandra et al. (2021), we perform a \log_2 transformation on the data and select the top 2.5% of genes with the highest variance. Subsequently, to normalize the dataset, similar to Subsection 6.1, we apply the CDF transformation (Liu et al., 2009) using the `bdgraph.npn()` function from the `BDgraph` R package. Detailed information on data processing, as well as the clean dataset, is available on the GitHub page³.

MCMC iterations are set to 60 million for RJ-MPL, 4 million for BD-MPL, 80,000 for BD, 3,000 for SS, and 500,000 for B-CONCORD, with half of the iterations considered burn-in. These values were chosen based on the results of the simulation study in Section 5. We adopt a Bernoulli prior for the graphical structure, assigning each edge a 1% inclusion probability, except for the B-CONCORD method, which defaults to a 50% prior edge inclusion probability. The rest of the initial parameter settings for running the algorithms were the same as those in the simulation study in Section 5.1 and the application in Subsection 6.1.

Figure 5 shows the number of edges in the visited graph for each algorithm over time. The RJ-MPL and BD-MPL algorithms converge the fastest, followed by SS and B-CONCORD. The BD algorithm did not yield meaningful results within a reasonable timeframe (over one day) and is excluded from further analysis in this section.

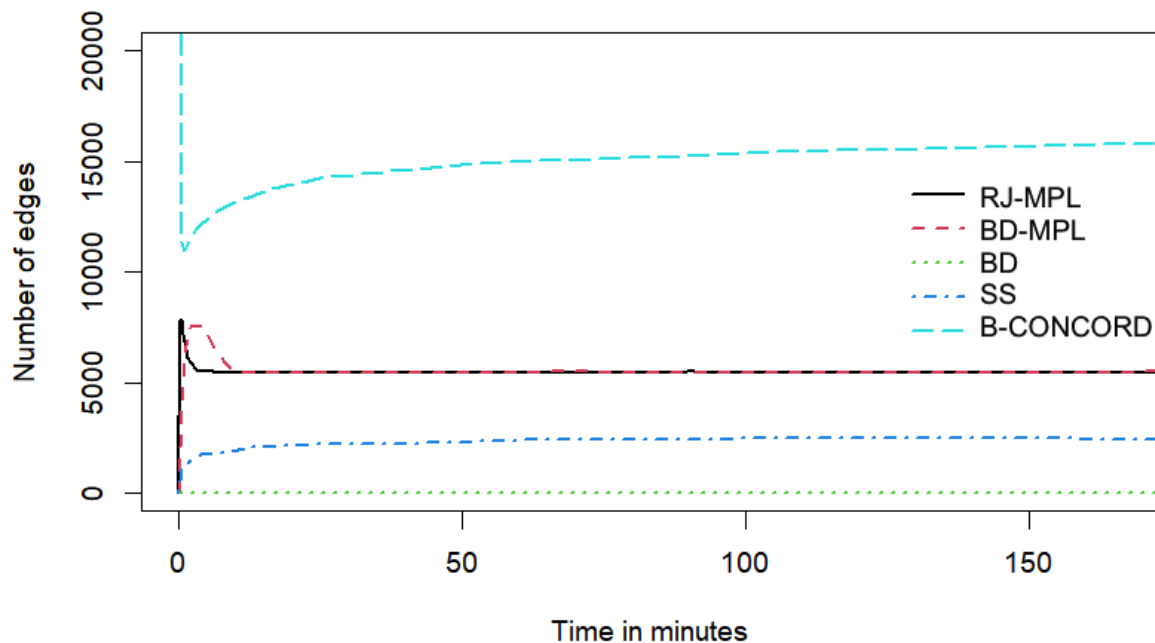


Figure 5: Plot tracking the number of edges in the Markov chain state over running time for each algorithm on the mice gene dataset ($p = 623$) to check convergence.

In this study, we refrain from presenting the final gene networks inferred by each algorithm due to the complex and dense nature of the estimated graphs. Instead, we focus

³<https://github.com/lucasvogels33/Large-scale-BSL-for-GGMs-using-MPL>

on specific gene subsets documented in the literature for their partial correlations. These subsets include histone genes (*e.g.*, *Hist1h1a*, *Hist1h1b*) (Wolffe, 2001), B-cell leukemia genes (*e.g.*, *Bcl2a1a*, *Bcl2a1b*) (Chandra et al., 2021), leukocyte antigen genes (*e.g.*, *Ly6c1*, *Ly6c2*) (Lee et al., 2013), and membrane-spanning 4A genes (*e.g.*, *Ms4a1*, *Ms4a4c*) (Liang et al., 2001). Figure 6 displays edges where the edge inclusion probability exceeds 0.99, illustrating that the BD-MPL and RJ-MPL algorithms effectively capture correlations among genes within these subsets.

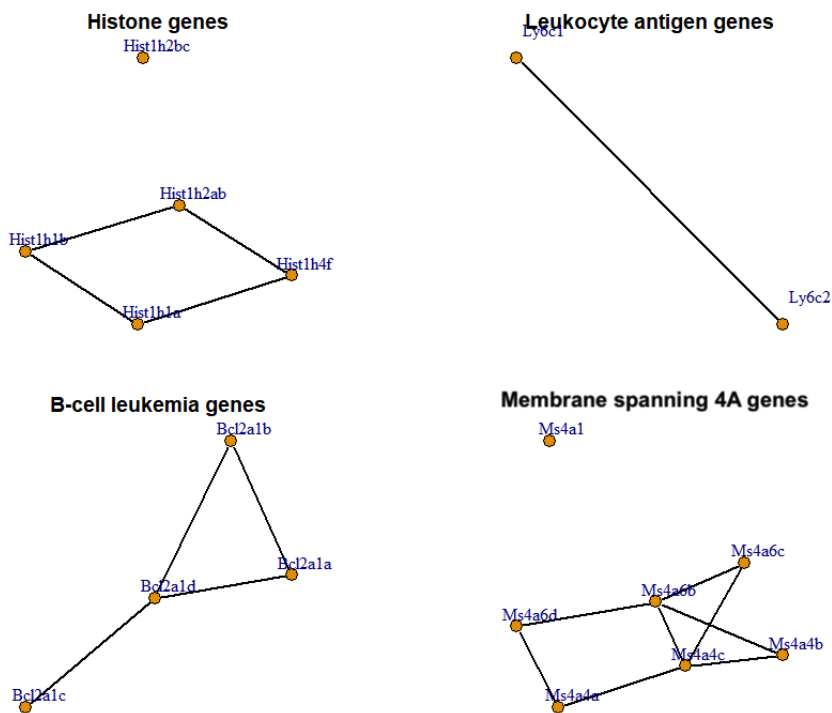


Figure 6: *The inferred gene networks for histone genes (Wolffe, 2001), leukocyte antigen genes (Lee et al., 2013), B-cell leukemia genes (Chandra et al., 2021), and membrane-spanning 4A genes (Liang et al., 2001) based on both the BD-MPL and RJ-MPL algorithms on the mice gene dataset ($p = 623$). All displayed edges exhibit edge inclusion probabilities exceeding 99%.*

Initially, the edge inclusion probabilities appear similar across algorithms, as indicated by the low average absolute differences between them, as shown in Table 6. However, these absolute differences are skewed due to the high sparsity of the graphs. The number of selected edges at a threshold of 0.9 varies significantly, as reported in Table 7: B-CONCORD identified 14,258 edges, RJ-MPL identified 4,282 edges, BD-MPL identified 3,965 edges, and SS identified 656 edges. The relatively dense estimate by the B-CONCORD method is likely due to its higher prior edge inclusion probability of 50%, compared to 1% for the other algorithms. Additionally, the relatively low sample size (n) may contribute to this difference. Table 7 also demonstrates substantial overlap in selected edges among the algorithms: SS selected between 91% and 96% of the edges identified by the other algorithms; RJ-MPL shares 70% of its selections with BD-MPL and 78% with B-CONCORD; and BD-MPL shares 80% of its selections with B-CONCORD.

	BD-MPL	RJ-MPL	SS	B-CONCORD
BD-MPL	-	0.019	0.026	0.071
RJ-MPL	-	-	0.026	0.072
SS	-	-	-	0.078
B-CONCORD	-	-	-	-

Table 6: Average absolute difference in edge inclusion probabilities across algorithms for the mice gene data set ($p = 623$).

	BD-MPL	RJ-MPL	SS	B-CONCORD
BD-MPL (3,965)	-	0.70	0.15	0.80
RJ-MPL (4,282)	0.65	-	0.14	0.78
SS (656)	0.92	0.91	-	0.96
B-CONCORD (14,258)	0.22	0.23	0.04	-

Table 7: Proportion of edges identified by the row algorithm that are also found by the column algorithm on the mice data set, using an edge inclusion probability threshold of 0.9. Between brackets is the number of edges with an edge inclusion probability higher than 0.9.

7 Conclusion

We introduced two novel MCMC-based search algorithms that integrate the birth-death and reversible jump algorithms with the marginal pseudo likelihood approach. These algorithms estimate the posterior distribution of the graph based on the data. This allows the exploration of the graph space instead of the joint space of graphs and precision matrices, leading to more efficient computational algorithms.

The proposed MCMC-based search algorithms (Algorithms 1 and 2) exhibit the following behavior: For relatively small-scale graphs ($p \in \{10, 100\}$ nodes), the proposed algorithms achieve similar or slightly lower AUC-PR values compared to state-of-the-art Bayesian structure learning methods (BD and SS). However, for large-scale graphs ($p = 1000$), the proposed algorithms can solve problems with high accuracy within minutes to hours. Specifically, for the *dense Cluster* graph with $p = 1000$ nodes and $n = 1050$ samples, the BD-MPL method achieves the highest AUC-PR value (greater than 0.7) in less than two hours, whereas the SS and B-CONCORD methods require over 27 hours, and the BD method takes over five days.

There are several promising lines of future research that could further enhance the performance of the proposed methods. First, the computational complexity of the BD-MPL method can be significantly reduced by leveraging parallel processing, particularly for calculating the birth and death rates (in Equation 13). Although Algorithm 1 is designed for parallel operations and is incorporated within the `BDgraph` package (Mohammadi et al., 2022), we chose not to employ its parallel capabilities to preserve the reproducibility of our simulation study and to align our methods with those of other algorithms. Another potential direction is to evaluate alternative priors for the precision matrix. In Section 3.1, we employ a non-informative prior to obtain a closed-form expression for the local fractional pseudo-likelihoods in Equation 8. As suggested by Leppä-aho et al. (2017) and Consonni and Rocca (2012), we use a non-informative improper prior; see, Jalali et al. (2020) for

an example using a spike-and-slab prior. Additionally, it may be worthwhile to investigate the possibility of multiple jumps within a single iteration to decrease computational time, explore alternative priors for the graph, or determine a suitable burn-in period.

Future research could integrate our Bayesian framework with variational inference (Wainwright et al., 2008) to further enhance computational efficiency and scalability in Bayesian structure learning for GGMs. Variational inference, a deterministic method for approximating posterior distributions through optimization, could significantly reduce computational complexity compared to MCMC methods. Pursuing this research direction could lead to faster convergence and the ability to handle larger data sets, while maintaining a balance between accuracy and computational resources.

SUPPLEMENTARY MATERIAL

R-package: The R package `BDgraph` contains code implementing our method described in this article. The BD-MPL and RJ-MPL algorithms are implemented in the function `bdgraph.mpl()`. The package is freely available from the Comprehensive R Archive Network (CRAN) at <http://cran.r-project.org/packages=BDgraph>.

GitHub repository: The code for reproducing all the results from our simulation study in Section 5 and our applications in Section 6, as well as instructions on how to download and process the data for analyses, is available on the GitHub page at <https://github.com/lucasvogels33/Large-scale-BSL-for-GGMs-using-MPL>.

Data sets: The data set used in Subsection 6.1 is available in the R package `BDgraph` (`geneExpression.RData` file). The data set used in Subsection 6.2 can be found on the GitHub page linked above (`cleaned_data.Rdata` file). Additionally, detailed information on data processing is provided on the GitHub page.

Supplementary materials: The supplementary materials provide additional results for the simulations presented in Section 5 of the manuscript. This includes convergence plots in Figure 7 and further graph recovery precision metrics: computational cost until AUC-ROC convergence in Table 8, AUC-ROC in Table 9, $F1$ in Table 10, Pr^+ in Table 11, and Pr^- in Table 12.

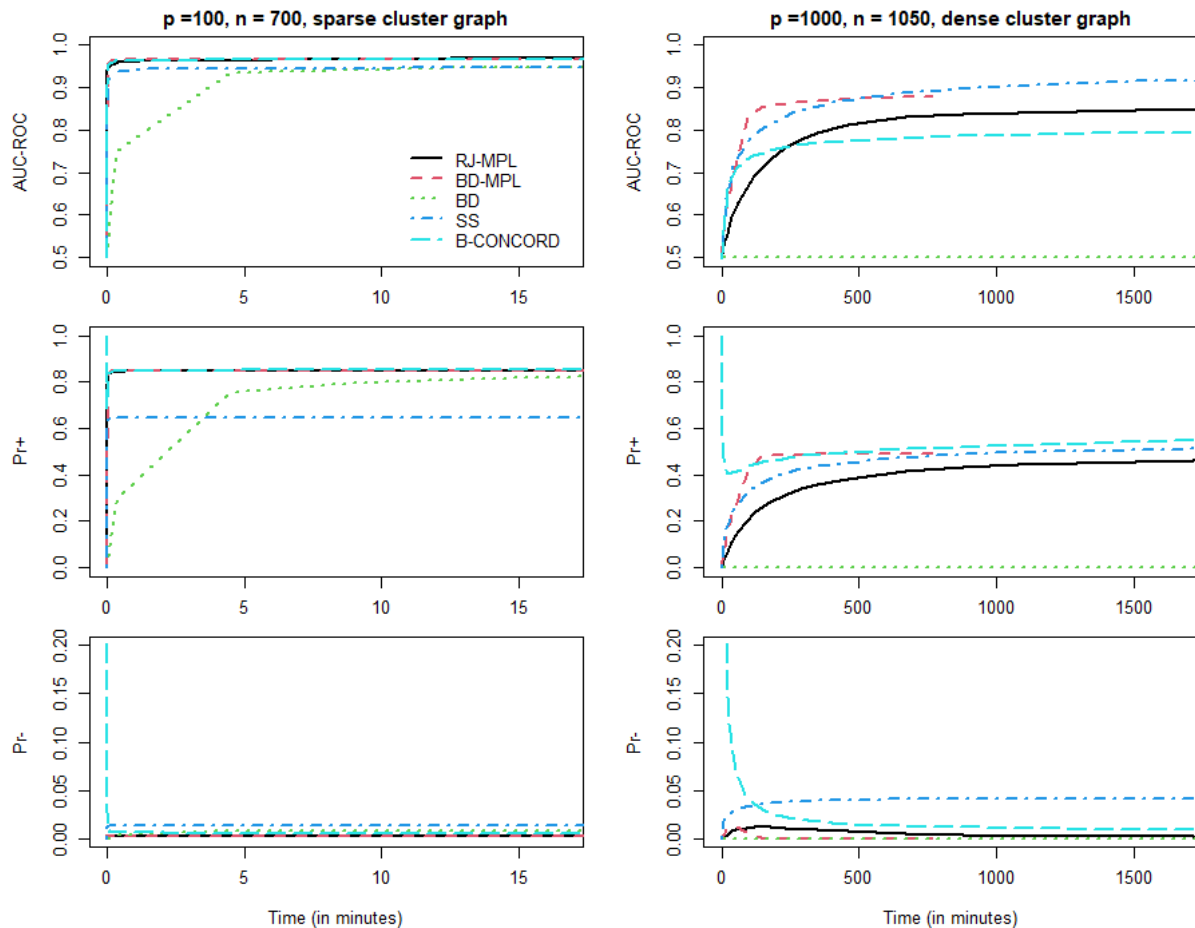


Figure 7: The convergence of AUC-ROC (top row), $Pr+$ (middle row), and $Pr-$ (bottom row) scores over running time for all algorithms (RJ-MPL, BD-MPL, BD, SS, B-CONCORD). The plots on the left represent the instance with $p = 100$, $n = 700$ for the sparse Cluster graph. The plots on the right represent the instance with $p = 1000$, $n = 1050$ for the dense Cluster graph.

References

- Albert, R. and A.-L. Barabási (2002). Statistical mechanics of complex networks. *Reviews of Modern Physics* 74(1), 47.
- Atay-Kayis, A. and H. Massam (2005). A Monte Carlo method for computing the marginal likelihood in nondecomposable Gaussian graphical models. *Biometrika* 92(2), 317–335.
- Atchadé, Y. F. (2019). Quasi-Bayesian estimation of large Gaussian graphical models. *Journal of Multivariate Analysis* 173, 656–671.
- Barbieri, M. M. and J. O. Berger (2004). Optimal predictive model selection. *Annals of Statistics*, 870–897.
- Besag, J. (1975). Statistical analysis of non-lattice data. *Journal of the Royal Statistical Society: Series D (The Statistician)* 24(3), 179–195.

- Bhadra, A. and B. Mallick (2013). Joint high-dimensional Bayesian variable and covariance selection with an application to eQTL analysis. *Biometrics* 69, 447–457.
- Cappé, O., C. Robert, and T. Rydén (2003). Reversible jump, birth-and-death and more general continuous time Markov chain Monte Carlo samplers. *Journal of the Royal Statistical Society: Series B (Statistical Methodology)* 65(3), 679–700.
- Carvalho, C. M. and J. G. Scott (2009). Objective Bayesian model selection in Gaussian graphical models. *Biometrika* 96(3), 497–512.
- Chandra, N. K., P. Mueller, and A. Sarkar (2021). Bayesian scalable precision factor analysis for massive sparse Gaussian graphical models. *arXiv preprint arXiv:2107.11316*.
- Cheng, Y. and A. Lenkoski (2012). Hierarchical Gaussian graphical models: Beyond reversible jump. *Electronic Journal of Statistics* 6, 2309–2331.
- Consonni, G. and L. L. Rocca (2012). Objective Bayes factors for Gaussian directed acyclic graphical models. *Scandinavian Journal of Statistics* 39(4), 743–756.
- Davis, J. and M. Goadrich (2006). The relationship between precision-recall and ROC curves. In *Proceedings of the 23rd International Conference on Machine Learning*, pp. 233–240.
- Desch, A., G. Randolph, K. Murphy, R. Kedl, M. Lahoud, I. Caminschi, K. Shortman, P. Henson, and C. Jakubzick (2011). CD103+ pulmonary dendritic cells preferentially acquire and present apoptotic cell-associated antigen. *The Journal of Experimental Medicine* 208, 1789–97.
- Dobra, A., A. Lenkoski, and A. Rodriguez (2011). Bayesian inference for general Gaussian graphical models with application to multivariate lattice data. *Journal of the American Statistical Association* 106(496), 1418–1433.
- Dobra, A. and R. Mohammadi (2018). Loglinear model selection and human mobility. *The Annals of Applied Statistics* 12(2), 815–845.
- Friedman, J., T. Hastie, and R. Tibshirani (2008). Sparse inverse covariance estimation with the graphical Lasso. *Biostatistics* 9(3), 432–441.
- Green, P. (1995). Reversible jump Markov chain Monte Carlo computation and Bayesian model determination. *Biometrika* 82(4), 711–732.
- Hanley, J. and B. Mcneil (1982). The meaning and use of the area under a receiver operating characteristic (roc) curve. *Radiology* 143(1), 29–36.
- Heng, T., M. Painter, K. Elpek, V. Lukacs-Kornek, N. Mauermann, S. Turley, D. Koller, F. Kim, A. Wagers, N. Asinovski, S. Davis, M. Fassett, M. Feuerer, D. Gray, S. Haxhinasto, J. Hill, G. Hyatt, C. Laplace, K. Leatherbee, and J. Kang (2008). The immunological genome project: Networks of gene expression in immune cells. *Nature Immunology* 9, 1091–1094.

- Hinne, M., A. Lenkoski, T. Heskes, and M. van Gerven (2014). Efficient sampling of Gaussian graphical models using conditional Bayes factors. *Stat* 3(1), 326–336.
- Jalali, P., K. Khare, and G. Michailidis (2020). B-CONCORD—a scalable Bayesian high-dimensional precision matrix estimation procedure. *arXiv preprint arXiv:2005.09017*.
- Jalali, P., K. Khare, and G. Michailidis (2023). A Bayesian subset specific approach to joint selection of multiple graphical models. *Statistica Sinica* 33, 1–24.
- Ji, C. and L. Seymour (1996). A consistent model selection procedure for Markov random fields based on penalized pseudolikelihood. *The Annals of Applied Probability* 6(2), 423–443.
- Jones, B., C. Carvalho, A. Dobra, C. Hans, C. Carter, and M. West (2005). Experiments in stochastic computation for high-dimensional graphical models. *Statistical Science* 20(4), 388–400.
- Khare, K., S.-Y. Oh, and B. Rajaratnam (2015). A convex pseudolikelihood framework for high dimensional partial correlation estimation with convergence guarantees. *Journal of the Royal Statistical Society: Series B (Statistical Methodology)* 77(4), 803–825.
- Koller, D. and N. Friedman (2009). *Probabilistic graphical models: Principles and techniques*. MIT Press.
- Lauritzen, S. L. (1996). *Graphical models*, Volume 17. Oxford: Oxford University Press.
- Lee, P. Y., J.-X. Wang, E. Parisini, C. C. Dascher, and P. A. Nigrovic (2013). Ly6 family proteins in neutrophil biology. *Journal of Leukocyte Biology* 94(4), 585–594.
- Lenkoski, A. (2013). A direct sampler for G-Wishart variates. *Stat* 2(1), 119–128.
- Lenkoski, A. and A. Dobra (2011). Computational aspects related to inference in Gaussian graphical models with the G-Wishart prior. *Journal of Computational and Graphical Statistics* 20, 140–157.
- Leppä-aho, J., Johan, T. Roos, and J. Corander (2017). Learning Gaussian graphical models with fractional marginal pseudo-likelihood. *International Journal of Approximate Reasoning* 83, 21–42.
- Letac, G. and H. Massam (2007). Wishart distributions for decomposable graphs. *The Annals of Statistics* 35(3), 1278–1323.
- Li, Y., B. A. Craig, and A. Bhadra (2019). The graphical horseshoe estimator for inverse covariance matrices. *Journal of Computational and Graphical Statistics* 28(3), 747–757.
- Liang, Y., T. R. Buckley, L. Tu, S. D. Langdon, and T. F. Tedder (2001). Structural organization of the human ms4a gene cluster on chromosome 11q12. *Immunogenetics* 53, 357–368.
- Liu, H., J. Lafferty, and L. Wasserman (2009). The nonparanormal: Semiparametric estimation of high dimensional undirected graphs. *Journal of Machine Learning Research* 10(80), 2295–2328.

- Meinshausen, N. and P. Bühlmann (2006). High-dimensional graphs and variable selection with the Lasso. *The Annals of Statistics* 34(3), 1436–1462.
- Mohammadi, A. and E. Wit (2015). Bayesian structure learning in sparse Gaussian graphical models. *Bayesian Analysis* 10(1), 109–138.
- Mohammadi, R. (2022). *ssgraph: Bayesian graph structure learning using spike-and-slab priors*. R package version 1.15.
- Mohammadi, R., H. Massam, and G. Letac (2023). Accelerating Bayesian structure learning in sparse Gaussian graphical models. *Journal of the American Statistical Association* 118(542), 1345–1358.
- Mohammadi, R., E. Wit, and A. Dobra (2022). *BDgraph: Bayesian structure learning in Graphical models using birth-death MCMC*. R package version 2.72.
- Mohammadi, R. and E. C. Wit (2019). BDgraph: An R package for Bayesian structure learning in graphical models. *Journal of Statistical Software* 89(3), 1–30.
- Niu, Y., Y. Ni, D. Pati, and B. K. Mallick (2023). Covariate-assisted Bayesian graph learning for heterogeneous data. *Journal of the American Statistical Association*, 1–15.
- Painter, M., S. Davis, R. Hardy, D. Mathis, and C. Benoist (2011). Transcriptomes of the B and T lineages compared by multiplatform microarray profiling. *Journal of Immunology (Baltimore, Md. : 1950)* 186, 3047–57.
- Peng, J., P. Wang, N. Zhou, and J. Zhu (2009). Partial correlation estimation by joint sparse regression models. *Journal of the American Statistical Association* 104(486), 735–746.
- Pensar, J., H. Nyman, J. Niiranen, and J. Corander (2017). Marginal pseudo-likelihood learning of discrete Markov network structures. *Bayesian Analysis* 12(4), 1195–1215.
- Peterson, C., F. C. Stingo, and M. Vannucci (2015). Bayesian inference of multiple Gaussian graphical models. *Journal of the American Statistical Association* 110(509), 159–174.
- Powers, D. M. (2020). Evaluation: from precision, recall and F-measure to ROC, informedness, markedness and correlation. *arXiv preprint arXiv:2010.16061*.
- Preston, C. J. (1976). Special birth-and-death processes. *Bulletin of the International Statistical Institute* 46, 371–391.
- Ravikumar, P., M. J. Wainwright, and J. D. Lafferty (2010). High-dimensional Ising model selection using ℓ_1 -regularized logistic regression. *The Annals of Statistics*, 1287–1319.
- Rothman, A. J., P. J. Bickel, E. Levina, and J. Zhu (2008). Sparse permutation invariant covariance estimation. *Electronic Journal of Statistics* 2, 494–515.
- Roverato, A. (2002). Hyper inverse Wishart distribution for non-decomposable graphs and its application to Bayesian inference for Gaussian graphical models. *Scandinavian Journal of Statistics* 29(3), 391–411.

- Rue, H. and L. Held (2005). *Gaussian Markov Random Fields: Theory and Applications*. London: Chapman and Hall-CRC Press.
- Sagar, K., S. Banerjee, J. Datta, and A. Bhadra (2024). Precision matrix estimation under the horseshoe-like prior–penalty dual. *Electronic Journal of Statistics* 18(1), 1–46.
- Scutari, M. (2013). On the prior and posterior distributions used in graphical modelling. *Bayesian Analysis* 8(3), 505–532.
- Stranger, B. E., A. C. Nica, M. S. Forrest, A. Dimas, C. P. Bird, C. Beazley, C. E. Ingle, M. Dunning, P. Flicek, D. Koller, S. Montgomery, S. Tavaré, P. Deloukas, and E. T. Dermitzakis (2007). Population genomics of human gene expression. *Nature Genetics* 39, 1217–1224.
- Tadesse, M. G. and M. Vannucci (2021). *Handbook of Bayesian variable selection*. CRC Press.
- Tierney, L. (1994). Markov chains for exploring posterior distributions. *The Annals of Statistics* 22(4), 1701 – 1728.
- Uhler, C., A. Lenkoski, and D. Richards (2018). Exact formulas for the normalizing constants of Wishart distributions for graphical models. *The Annals of Statistics* 46(1), 90–118.
- van den Boom, W., A. Beskos, and M. De Iorio (2022). The G-Wishart weighted proposal algorithm: Efficient posterior computation for Gaussian graphical models. *Journal of Computational and Graphical Statistics* 31(4), 1215–1224.
- Varin, C., N. Reid, and D. Firth (2011). An overview of composite likelihood methods. *Statistica Sinica*, 5–42.
- Vogels, L., R. Mohammadi, M. Schoonhoven, and Ş. İ. Birbil (2023). Bayesian structure learning in undirected Gaussian graphical models: Literature review with empirical comparison. *arXiv preprint arXiv:2307.02603*.
- Wainwright, M. J., M. I. Jordan, et al. (2008). Graphical models, exponential families, and variational inference. *Foundations and Trends® in Machine Learning* 1(1–2), 1–305.
- Wang, H. (2012). The Bayesian graphical Lasso and efficient posterior computation. *Bayesian Analysis* 7, 771–790.
- Wang, H. (2015). Scaling it up: Stochastic search structure learning in graphical models. *Bayesian Analysis* 10, 351–377.
- Wang, H. and S. Li (2012). Efficient Gaussian graphical model determination under G-Wishart prior distributions. *Electronic Journal of Statistics* 6, 168–198.
- Wolffe, A. (2001). Histone genes. In S. Brenner and J. H. Miller (Eds.), *Encyclopedia of Genetics*, pp. 948–952. New York: Academic Press.
- Zanella, G. (2020). Informed proposals for local MCMC in discrete spaces. *Journal of the American Statistical Association* 115(530), 852–865.

p	Graph	Density	n	RJ-MPL	BD-MPL	BD	SS	B-CONCORD	
1000	Random	Sparse	400	1287	45	-	321	664	
		Sparse	1050	851	79	-	328	338	
		Dense	400	2581	499	-	2097	3528	
		Dense	1050	2125	901	-	2122	1752	
	Cluster	Sparse	400	1374	38	-	301	633	
		Sparse	1050	874	71	-	318	240	
		Dense	400	2429	480	-	2111	1626	
		Dense	1050	2160	402	-	1791	916	
	Scale-free	Sparse	400	2143	19	-	387	595	
		Sparse	1050	1173	38	-	1086	67	
	100	Random	Sparse	40	1	2	63	0	3
			Sparse	700	1	0	31	0	0
Dense			40	4	1	89	1	4	
Dense			700	3	0	50	1	1	
Cluster		Sparse	40	2	1	60	0	3	
		Sparse	700	1	1	49	5	0	
		Dense	40	4	1	107	0	3	
		Dense	700	2	1	54	1	1	
Scale-free		Sparse	40	5	4	85	0	3	
		Sparse	700	3	0	54	3	0	
10		Random	Sparse	20	0	0	0	0	0
			Sparse	350	0	0	0	0	0
	Dense		20	0	0	0	0	0	
	Dense		350	0	0	0	0	0	
	Cluster	Sparse	20	0	0	0	0	0	
		Sparse	350	0	0	0	0	0	
		Dense	20	0	0	0	0	0	
		Dense	350	0	0	0	0	0	
	Scale-free	Sparse	20	0	0	0	0	0	
		Sparse	350	0	0	0	0	0	

Table 8: Computational cost (T) in minutes until AUC-ROC convergence for different instances. T represents the average time until AUC-PR convergence, based on 16 replications for $p \in \{10, 100\}$ and 8 replications for $p = 1000$. A “-” indicates that an algorithm did not converge within five days. The best methods are highlighted in bold.

p	Graph	Density	n	RJ-MPL	BD-MPL	BD	SS	B-CONCORD	
1000	Random	Sparse	400	0.87	0.89	0.50	0.90	0.89	
		Sparse	1050	0.91	0.92	0.50	0.92	0.94	
		Dense	400	0.70	0.74	0.50	0.76	0.70	
		Dense	1050	0.77	0.80	0.50	0.83	0.78	
	Cluster	Sparse	400	0.88	0.90	0.50	0.90	0.90	
		Sparse	1050	0.92	0.93	0.50	0.92	0.94	
		Dense	400	0.78	0.84	0.50	0.89	0.72	
		Dense	1050	0.86	0.88	0.50	0.93	0.80	
	Scale-free	Sparse	400	0.89	0.90	0.50	0.92	0.91	
		Sparse	1050	0.93	0.93	0.50	0.93	0.95	
	100	Random	Sparse	40	0.85	0.86	0.86	0.87	0.86
			Sparse	700	0.97	0.97	0.97	0.96	0.97
Dense			40	0.75	0.75	0.75	0.77	0.76	
Dense			700	0.94	0.94	0.94	0.92	0.94	
Cluster		Sparse	40	0.85	0.85	0.84	0.85	0.85	
		Sparse	700	0.97	0.97	0.96	0.95	0.97	
		Dense	40	0.77	0.77	0.77	0.79	0.77	
		Dense	700	0.94	0.95	0.95	0.92	0.94	
Scale-free		Sparse	40	0.81	0.80	0.82	0.84	0.81	
		Sparse	700	0.95	0.95	0.96	0.95	0.95	
10		Random	Sparse	20	0.80	0.80	0.80	0.78	0.75
			Sparse	350	0.95	0.96	0.96	0.92	0.94
	Dense		20	0.68	0.68	0.69	0.68	0.68	
	Dense		350	0.92	0.92	0.92	0.91	0.90	
	Cluster	Sparse	20	0.73	0.75	0.75	0.75	0.74	
		Sparse	350	0.90	0.91	0.91	0.90	0.92	
		Dense	20	0.81	0.81	0.82	0.79	0.75	
		Dense	350	0.94	0.94	0.95	0.92	0.92	
	Scale-free	Sparse	20	0.76	0.76	0.78	0.79	0.76	
		Sparse	350	0.92	0.94	0.94	0.92	0.92	

Table 9: $AUC - ROC$ scores of the algorithms for different instances. The $AUC - PR$ reaches its best score at 1 and its worst at 0. The values are averages over 16 replications for $p \in \{10, 100\}$ and over 8 replications for $p = 1000$. The best methods are highlighted in bold.

p	Graph	Density	n	RJ-MPL	BD-MPL	BD	SS	B-CONCORD	
1000	Random	Sparse	400	0.73	0.73	0.00	0.68	0.65	
		Sparse	1050	0.84	0.84	0.00	0.75	0.72	
		Dense	400	0.40	0.40	0.00	0.39	0.40	
		Dense	1050	0.59	0.60	0.00	0.55	0.56	
	Cluster	Sparse	400	0.75	0.75	0.00	0.69	0.70	
		Sparse	1050	0.85	0.85	0.00	0.76	0.75	
		Dense	400	0.47	0.47	0.00	0.47	0.55	
		Dense	1050	0.65	0.65	0.00	0.63	0.67	
	Scale-free	Sparse	400	0.62	0.62	0.00	0.63	0.49	
		Sparse	1050	0.75	0.75	0.00	0.79	0.53	
	100	Random	Sparse	40	0.41	0.41	0.54	0.57	0.52
			Sparse	700	0.85	0.84	0.89	0.75	0.79
Dense			40	0.38	0.38	0.42	0.37	0.39	
Dense			700	0.85	0.85	0.86	0.65	0.79	
Cluster		Sparse	40	0.44	0.44	0.52	0.54	0.51	
		Sparse	700	0.83	0.83	0.87	0.75	0.78	
		Dense	40	0.40	0.39	0.42	0.39	0.41	
		Dense	700	0.85	0.85	0.86	0.69	0.81	
Scale-free		Sparse	40	0.41	0.41	0.50	0.48	0.46	
		Sparse	700	0.86	0.86	0.89	0.70	0.73	
10		Random	Sparse	20	0.40	0.40	0.36	0.27	0.33
			Sparse	350	0.9	0.9	0.89	0.55	0.90
	Dense		20	0.37	0.37	0.33	0.24	0.33	
	Dense		350	0.84	0.84	0.83	0.6	0.84	
	Cluster	Sparse	20	0.43	0.43	0.35	0.19	0.38	
		Sparse	350	0.83	0.84	0.82	0.60	0.82	
		Dense	20	0.44	0.44	0.41	0.28	0.37	
		Dense	350	0.81	0.81	0.81	0.69	0.84	
	Scale-free	Sparse	20	0.47	0.47	0.49	0.33	0.41	
		Sparse	350	0.88	0.88	0.88	0.66	0.83	

Table 10: $F1$ scores (at a threshold of 0.5) of the algorithms for different instances. The $F1$ score reaches its best score at 1 and its worst at 0. The values are averages over 16 replications for $p \in 10, 100$ and over 8 replications for $p = 1000$. The best methods are highlighted in bold.

p	Graph	Density	n	RJ-MPL	BD-MPL	BD	SS	B-CONCORD	
1000	Random	Sparse	400	0.63	0.65	0.00	0.62	0.67	
		Sparse	1050	0.74	0.76	0.00	0.64	0.78	
		Dense	400	0.26	0.26	0.00	0.31	0.34	
		Dense	1050	0.41	0.44	0.00	0.44	0.51	
	Cluster	Sparse	400	0.64	0.66	0.00	0.64	0.69	
		Sparse	1050	0.75	0.78	0.00	0.66	0.8	
		Dense	400	0.31	0.32	0.00	0.38	0.42	
		Dense	1050	0.48	0.49	0.00	0.53	0.56	
	Scale-free	Sparse	400	0.70	0.70	0.00	0.68	0.70	
		Sparse	1050	0.80	0.81	0.00	0.68	0.81	
	100	Random	Sparse	40	0.54	0.54	0.53	0.50	0.52
			Sparse	700	0.87	0.87	0.86	0.65	0.87
Dense			40	0.30	0.30	0.33	0.28	0.29	
Dense			700	0.75	0.75	0.77	0.52	0.78	
Cluster		Sparse	40	0.54	0.54	0.52	0.49	0.52	
		Sparse	700	0.85	0.85	0.84	0.64	0.85	
		Dense	40	0.31	0.31	0.34	0.30	0.30	
		Dense	700	0.75	0.75	0.78	0.55	0.78	
Scale-free		Sparse	40	0.40	0.41	0.43	0.38	0.38	
		Sparse	700	0.82	0.82	0.83	0.56	0.81	
10		Random	Sparse	20	0.36	0.36	0.31	0.24	0.25
			Sparse	350	0.84	0.84	0.82	0.44	0.83
	Dense		20	0.28	0.28	0.26	0.19	0.21	
	Dense		350	0.73	0.73	0.73	0.49	0.75	
	Cluster	Sparse	20	0.36	0.36	0.30	0.21	0.26	
		Sparse	350	0.74	0.75	0.73	0.46	0.74	
		Dense	20	0.32	0.32	0.3	0.23	0.25	
		Dense	350	0.69	0.69	0.69	0.55	0.73	
	Scale-free	Sparse	20	0.37	0.37	0.36	0.26	0.29	
		Sparse	350	0.79	0.79	0.79	0.53	0.78	

Table 11: Pr^+ scores of the algorithms for different instances. The Pr^+ reaches its best score at 1 and its worst at 0. The values are averages over 16 replications for $p \in \{10, 100\}$ and over 8 replications for $p = 1000$. The best methods are highlighted in bold.

p	Graph	Density	n	RJ-MPL	BD-MPL	BD	SS	B-CONCORD	
1000	Random	Sparse	400	0.00	0.00	0.00	0.03	0.01	
		Sparse	1050	0.00	0.00	0.00	0.02	0.01	
		Dense	400	0.00	0.00	0.00	0.06	0.02	
		Dense	1050	0.00	0.00	0.00	0.05	0.02	
	Cluster	Sparse	400	0.00	0.00	0.00	0.03	0.01	
		Sparse	1050	0.00	0.00	0.00	0.02	0.00	
		Dense	400	0.00	0.00	0.00	0.05	0.01	
		Dense	1050	0.00	0.00	0.00	0.04	0.01	
	Scale-free	Sparse	400	0.00	0.00	0.00	0.03	0.01	
		Sparse	1050	0.00	0.00	0.00	0.02	0.01	
	100	Random	Sparse	40	0.02	0.02	0.04	0.04	0.01
			Sparse	700	0.00	0.00	0.01	0.01	0.01
Dense			40	0.02	0.02	0.05	0.05	0.01	
Dense			700	0.00	0.00	0.01	0.02	0.01	
Cluster		Sparse	40	0.02	0.02	0.03	0.04	0.01	
		Sparse	700	0.00	0.00	0.01	0.01	0.01	
		Dense	40	0.02	0.02	0.05	0.05	0.01	
		Dense	700	0.00	0.00	0.01	0.02	0.01	
Scale-free		Sparse	40	0.02	0.02	0.04	0.04	0.01	
		Sparse	700	0.00	0.00	0.01	0.01	0.01	
10		Random	Sparse	20	0.04	0.04	0.05	0.04	0.01
			Sparse	350	0.01	0.01	0.01	0.01	0.01
	Dense		20	0.07	0.07	0.09	0.07	0.05	
	Dense		350	0.01	0.01	0.03	0.02	0.03	
	Cluster	Sparse	20	0.05	0.05	0.05	0.04	0.02	
		Sparse	350	0.01	0.01	0.01	0.01	0.01	
		Dense	20	0.04	0.04	0.05	0.04	0.00	
		Dense	350	0.00	0.00	0.01	0.02	0.01	
	Scale-free	Sparse	20	0.05	0.05	0.06	0.05	0.02	
		Sparse	350	0.01	0.01	0.02	0.01	0.03	

Table 12: Pr^- scores of the algorithms for different instances. The Pr^- reaches its best score at 0 and its worst at 1. The values are averages over 16 replications for $p \in \{10, 100\}$ and over 8 replications for $p = 1000$. The best methods are highlighted in bold.

p	Graph	Density	n	RJ-MPL	BD-MPL	BD	SS	B-CONCORD	
1000	Random	Sparse	400	16000K	300K	10	600	40K	
		Sparse	1050	16000K	200K	10	400	40K	
		Dense	400	30000K	1500K	10	1500	250K	
		Dense	1050	10000K	500K	10	1500	80K	
	Cluster	Sparse	400	16000K	300K	10	600	40K	
		Sparse	1050	16000K	200K	10	400	40K	
		Dense	400	30000K	1500K	10	1500	250K	
		Dense	1050	30000K	500K	10	1500	80K	
	Scale-free	Sparse	400	30000K	200K	10	600	50K	
		Sparse	1050	30000K	200K	10	200	50K	
	100	Random	Sparse	40	125000K	2500K	30K	45K	400K
			Sparse	700	125000K	2500K	30K	45K	400K
Dense			40	125000K	2500K	30K	45K	400K	
Dense			700	125000K	2500K	30K	45K	400K	
Cluster		Sparse	40	125000K	2500K	30K	45K	400K	
		Sparse	700	125000K	2500K	30K	45K	400K	
		Dense	40	125000K	2500K	30K	45K	400K	
		Dense	700	125000K	2500K	30K	45K	400K	
Scale-free		Sparse	40	125000K	2500K	30K	45K	400K	
		Sparse	700	125000K	2500K	30K	45K	400K	
10		Random	Sparse	20	100K	30K	30K	3K	10K
			Sparse	350	100K	30K	30K	3K	10K
	Dense		20	100K	30K	30K	3K	10K	
	Dense		350	100K	30K	30K	3K	10K	
	Cluster	Sparse	20	100K	30K	30K	3K	10K	
		Sparse	350	100K	30K	30K	3K	10K	
		Dense	20	100K	30K	30K	3K	10K	
		Dense	350	100K	30K	30K	3K	10K	
	Scale-free	Sparse	20	100K	30K	30K	3K	10K	
		Sparse	350	100K	30K	30K	3K	10K	

Table 13: Number of MCMC iterations until AUC-PR convergence for different instances. The time limit was set to five days, which is why the number of iterations for the BD algorithm for cases with $p = 1000$ is only 10.